Heliyon 10 (2024) e37722

Contents lists available at ScienceDirect

Heliyon

journal homepage: www.cell.com/heliyon

Spectrochip-based Calibration Curve Modeling (CCM) for Rapid and Accurate Multiple Analytes Quantification in Urinalysis

Cheng-Hao Ko [a,b,*], Ashenafi Belihu Tadesse [a], Abel Chernet Kabiso [a]

[a] Graduate Institute of Automation and Control, National Taiwan University of Science and Technology, Taipei, Taiwan
[b] Spectrochip Inc., Hsinchu, Taiwan

ARTICLE INFO

Keywords:
Characteristic Wavelength (λ_c)
Calibration Curve Modeling (CCM)
Micro-electromechanical System (MEMS)
Point-of-Care (POC) Testing
Spectrochip
Urinalysis

ABSTRACT

Most urine test strips are intended to enable the general population to rapidly and easily diagnose potential renal disorders. It is semi-quantitative in nature, and although the procedure is straightforward, certain factors will affect the judgmental outcomes. This study describes rapid and accurate quantification of twelve urine test strip parameters: leukocytes, nitrite, urobilinogen, protein, pH, occult blood, specific gravity, ketone, bilirubin, glucose, microalbumin, and creatinine using a micro-electromechanical system (MEMS)-based spectrophotometer, known as a spectrochip. For each parameter, absorption spectra were measured three times independently at eight different concentration levels of diluted standard solutions, and the average spectral intensities were calculated to establish the calibration curve under the characteristic wavelength (λ_c). Then, regression analysis on the calibration curve was performed with GraphPad Prism software, which revealed that the coefficient of determination (R^2) of the modeled calibration curves was greater than 0.95. This result illustrates that the measurements exceed standard levels, confirming the importance of a spectrochip for routine multi-parameter urine analysis. Thus, it is possible to obtain the spectral signal strength for each parameter at its characteristic wavelength in order to compare directly with the calibration curves in the future, even in situations when sample concentration is unknown. Additionally, the use of large testing machines can be reduced in terms of cost, time, and space by adopting a micro urine testing platform based on spectrochip, which also improves operational convenience and effectively enables point-of-care (POC) testing in urinalysis.

1. Introduction

Urine, a metabolic by-product excreted by vertebrates, plays a crucial role in maintaining electrolyte and water balance and removing waste products. Healthy adults typically excrete 1500 - 2500 ml of urine daily with a pH of 6.5 to 7 [1]. Urinalysis is used to evaluate the health of the kidneys and other organs within the urinary system. The normal urine color appearing clear to pale yellow with no impurities [2]. Such test can detects abnormalities, including the presence of red blood cells signaling occult blood [3], or increased creatinine levels from conditions like rhabdomyolysis, which causes urine to appear tea-colored [4], [5]. Routine urine tests involve urine sediment microscopy, which, despite its accuracy, requires sophisticated equipment and trained medical personnel, making it unsuitable for rapid testing [6]. Alternatively, urine test strips offer a quicker, albeit less comprehensive, diagnostic method

* Corresponding author. Graduate Institute of Automation and Control, National Taiwan University of Science and Technology, Taipei, Taiwan.
E-mail address: kevin.ko.ntust.2@gmail.com (C.-H. Ko).

https://doi.org/10.1016/j.heliyon.2024.e37722
Received 28 May 2024; Received in revised form 6 September 2024; Accepted 9 September 2024
Available online 12 September 2024

by indicating chemical composition changes in urine, such as the presence of red or white blood cells, proteins, ketones, creatinine, and sugar, which suggest deviations from normal levels [7]. Moreover, variations in individual color sensitivity can lead to errors when using visual comparison methods with a color card for concentration analysis [8]. This underscores the importance of using a device, like spectrophotometer, for a precise and prompt diagnostic results.

Analytical chemistry utilizes classical (i.e., chemical reactions) and instrumental analysis techniques to assess chemical properties; the latter measures physical properties for a more sensitive, accurate, and rapid assessment of chemical composition, concentration, molecular, and atomic structures [9], [10]. Common methods in instrumental analysis include: spectroscopy, chromatography, electrochemical analysis, and colorimetry [11], [12], [13], [14], [15]. Each method was applied in a variety of scientific disciplines widely and intensely, including toxicity [16], [17], [18], [19]; food analysis [20], [21], [22], [23]; pharmaceutical research [24], [25], [26], [27], [28], [29]; water quality monitoring [30], [31], [32], [33], [34], [35]; astronomical observations [36], [37], [38]. Spectroscopy, which analyzes the interaction between electromagnetic radiation and matter (i.e., emission, absorption, or scattering), employs spectrometers to dissect light into its spectral lines, allowing precise material identification despite its operational challenges [9], [39].

Recent advancements in photo-electrochemical (PEC) sensing and chemiluminescence-derived PEC immunoassays have significantly advanced instrumental analysis. Using light and cutting-edge materials, such as nanostructured anodic TiO2 and quantum dots (QDs), PEC sensors achieve high sensitivity and specificity in detecting substances like glucose [40], [41], [42]. These innovations are enhanced by integrating optical fibers and selective films such as Nafion, broadening their use from molecular to immunochemical applications [43], [44], [45], [46]. Moreover, chemiluminescence in PEC immunoassays generates self-sustaining electrical signals for target binding, facilitating power-independent diagnostics and enhancing the detection and quantification of scarce disease-related proteins [47], [48], [49]. These systems benefit from interdisciplinary advancements that combine physics, biology, and chemistry, creating cost-effective, user-friendly, and highly accurate diagnostic tools [47], [48]. The integration of optical multisensor systems further improves the real-time, in-line analysis, ensuring the reliability and reproducibility of analytical data and meeting the precise demands of life and environmental sciences [50], [51]. These innovations ensure the reliability and reproducibility of analytical data, meeting the growing demands of life sciences and environmental sciences for higher precision [52], [47], [43], [49].

Now a day, along with the development of MEMS, diagnostic devices have become increasingly compact (i.e., small, but complete [53]), which have dramatically enhanced POC testing, reducing reliance on centralized laboratories by enabling rapid, accurate diagnostics directly at the site of patient care [54], [55]. Systems, like integrated solar-powered PEC immunoassays for detecting cardiac troponin I (cTnI) using advanced microfabrication techniques and portable photothermal immunosensing platforms for detecting aflatoxin B1 (AFB_1) in food, which demonstrates the ability of MEMS to deliver rapid, sensitive, efficient, and on-site diagnostics in various settings, including resource-limited environments [56]. Further, combining MEMS with technologies, like surface acoustic wave (SAW) biochips, has led to ultra-rapid HIV detection devices, facilitating immediate clinical decisions [57]. These technologies not only expedite diagnostics in fields ranging from infectious disease to food safety, but also improve clinical and economic outcomes by providing faster results than conventional methods [58], [59], [60]. Despite these advancements, challenges such as technical limitations and personnel training remain, highlighting the need for ongoing development and quality assurance [61], [62]. Overall, the integration of MEMS into POC testing significantly advances the capability for rapid and reliable diagnostics, ultimately enhancing patient care and public health [63] [64], [65].

This study has successfully demonstrated the use of a MEMS-based micro-spectrometer, known as Spectrochip, for the precise quantification of twelve critical urine test parameters: leukocytes, nitrite, urobilinogen, protein, pH, occult blood, specific gravity, ketone, bilirubin, glucose, microalbumin, and creatinine. By integrating both ten-items and microalbuminuria test strips, as shown in Fig. S1., with the Spectrochip, we developed a micro-urine analyzer that not only captures characteristic wavelengths (λ_c) from the absorption spectra of these biomarkers but also establishes calibration curves to simplify the diagnosis of abnormalities. The ability of this system to deliver rapid, accurate, and reproducible diagnostics directly at the point of care marks a significant advancement in the field of clinical urinalysis. This research underscores the potential of MEMS technology in enhancing the efficiency and effectiveness of medical diagnostics, paving the way for future innovations that could further revolutionize healthcare practices.

2. Biomarkers Clinical Implications

In urinalysis, several key biomarkers were investigated for their physiological roles and pathological significances, and implications for health. In this study, we examine specific urine biomarkers crucial for diagnosing and monitoring various health conditions. The studied biomarkers include leukocytes, nitrite, urobilinogen, protein, pH, occult blood, specific gravity, ketone, bilirubin, glucose, microalbumin, and creatinine. This section will detail the physiological significance of each biomarker, their roles in health and disease, and the methods used for their analysis. **Leukocytes**, or white blood cells (WBC), are part of the immune system, which can suggest urinary tract infection (UTI) or kidney stones when present in urine, known as leukocyturia [66], [67]. Urine normally doesn't contain **nitrite**. It manifests when the urinary system is infected with bacteria that can convert dietary nitrates to nitrites. The presence of nitrite in urine is a strong indicator of a bacterial UTI, making this test a valuable tool for quick infection screening [68], [69], [70]. **Urobilinogen** is produced in the intestines from the breakdown of bilirubin and is usually excreted in the feces. It is part of the body's process of breaking down and eliminating old red blood cells. Elevated levels of this compound in urine can indicate liver diseases such as hepatitis or cirrhosis, or conditions causing increased red blood cell breakdown, such as hemolytic anemia [71]. **Proteins** in urine, particularly albumin, can indicate kidney damage when found in significant amounts. This condition, known as proteinuria (physiological and pathological), might be due to a variety of causes, including consuming excessive high-protein foods, engaging in intense physical activities, kidney disease, high blood pressure, or diabetes. Measuring protein levels helps in assessing kidney function and

guiding treatment decisions [72]. The **pH** of urine is determined by the kidney's excretion of hydrogen ions. It reflects the kidney's ability to maintain the body's acid-base balance. Abnormal urine pH levels might indicate kidney stones, UTI, or systemic conditions (i.e., metabolic or respiratory acidosis or alkalosis) [73]. **Occult blood** in urine indicates the presence of red blood cells, known as hematuria. It can be a sign of serious conditions such as UTI, kidney stones, tumors, or kidney disease. Detecting occult blood in urine is critical for diagnosing these underlying diseases early, however vitamin-C and menstruation causing results false positives [74], [75].

Specific gravity measures urine density compared to water, which reflects solute concentration in the urine. Thus, it indicates the kidney's ability to concentrate or dilute urine based on the body's hydration needs. Abnormal specific gravity readings can suggest dehydration, overhydration, or kidney disorders that impair the kidneys' concentrating ability [76], [77], [78]. **Ketones** are byproducts of fat metabolism, typically appearing in urine when the body burns fat for providing energy to the tissues in the brain, heart, muscle, and kidney in the conditions of glucose insufficiency and uncontrolled diabetes. This occurs during prolonged fasting, carbohydrate restrictive diets, or uncontrolled diabetes, particularly diabetic ketoacidosis, a potentially life-threatening condition [79], [80], [81]. Under normal conditions, **bilirubin**, which is originates from the breakdown of hemoglobin in red blood cells, is not found in urine. However, its presence may indicate liver dysfunction, such as hepatitis, cirrhosis, or bile duct obstruction. Testing for bilirubin in urine is crucial for the early detection and treatment of liver-related diseases [71]. **Glucose** should be reabsorbed in the kidneys and not appear in urine. Its presence, known as glycosuria, is a common sign of diabetes mellitus or renal glycosuria, where high blood sugar levels lead to glucose spilling into the urine. Testing for glucose can assist in diagnosing and monitoring of diabetes and other diseases, such as hyperthyroidism and pancreatitis [82]. **Microalbumin** test detects small amounts of albumin protein in urine. Small amounts may be normally excreted by the kidneys; however significant levels are abnormal. Microalbuminuria is an early sign of kidney damage, especially in the context of diabetes, and it may lead to significant proteinuria. Regular testing is crucial for diabetic patients to monitor kidney health earlier. **Creatinine** is a waste product from normal muscle metabolism, consistently produced by the body and excreted at stable rate by the kidneys. The normal range for creatinine in the human body is 0.7 to 1.2 mg/dl for men and 0.6 to 1.1 mg/dl for women, however the values are higher in males and in individuals, such as athletes and meat eaters [83], [84]. Measuring creatinine levels in urine are used to assess kidney function and essential for interpreting other urine test results, like albumin-to-creatinine ratio (ACR) and glomerular filtration rate (GFR). ACR helps to evaluate glomerular pathology, adjusting for urine concentration variations [72], [85], [86].

$$GFR = 186 \cdot creatinine^{-1.154} \cdot Age^{-0.203} \tag{1}$$

Equation (1) is the most widely used GFR formula derived by the United States Modification of Diet in Renal Disease (MDRD) [87] and adjusted for body surface area (in $ml/min/1.73\ m^2$), uses a 0.742 factor for females and 1.210 factor for black Africans to classify five CKD stages, as depicted in **Table-S1** [88], [89]. Typically, kidney disease appears with no symptoms in the early stages of renal function decline [90], [91], [92]. Utilizing advanced micro-spectrometry techniques, we quantify these parameters to improve diagnostic accuracy and deepen our understanding of related diseases such as diabetes, kidney disease, and urinary tract infections.

3. Materials and Method

3.1. Study Procedure

To ensure the accuracy and reliability of the study, various actions has been implemented, as depicted in Figure 1. Firstly, the stability of the system needs to be verified to ensure consistent and reproducible measurement system. Next, the stability of the test paper itself should be verified to confirm that it provides consistent responses over time. Following this, standard solutions of known concentrations need to be prepared carefully to serve as reference points for calibration. These standard solutions are then subjected to three repeated independent measurements to assess measurement precision and reliability. Subsequently, characteristic wavelengths are identified from average absorption spectra of the standard solution, and a calibration curve is established using these selected wavelengths. Finally, the coefficient of determination (R^2) is calculated to evaluate the goodness of fit of the calibration curve and its predictive power through regression analysis using GraphPad Prism. By rigorously following these procedures, a robust and accurate calibration curve can be developed for precise measurement and analysis of a given standard solution.

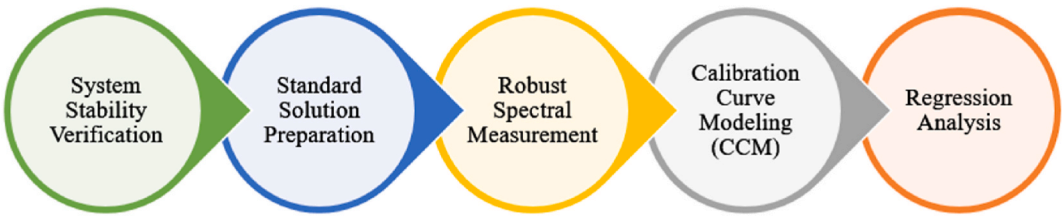

Figure 1. Conceptual framework of the study.

3.2. Materials

Urine Test Strips

For this study, Ten Parameter Urine Test Strips and Microalbumin Urine Test strips (Microalbumin and Creatinine) were used, as shown in Fig. S1., which can detect ten standard urine parameters and creatinine with microalbumin, respectively. The results of the measurements can provide insight into renal disorders in their early stages and other associated ailments.

Spectrochip

As shown in Figure 2(a), the spectrometer can be modularized into a spectral chip module using an image sensor and a MEMS-based manufacturing process, known as the Micro-Grating Process. The modular design can be fitted onto CNC-machined parts to suit different biomedical measurement requirements. Table 1 summarizes the specifications spectral chip module. Figure 2(b) shows the overall spectrochip micro urine analysis device assembly.

Light Source

Stability, cost size, durability and wavelength range are the major criteria for selecting the preferable light source for the system. White light LEDs have a limited wavelength range of 400 to 700 nm [93], but they have benefits including consistent emission, low cost, compact size, and a lifespan of up to 100,000 hours. Hence, the Cree XLamp XT-E White light source was used for this setup.

3.3. Optical Platform Calibration

The distance between the center and the edge of each of the twelve test strips must be measured with a Vernier caliper prior to beginning the measurements, which is crucial for identifying the exact region of interest (ROI). Then, by using the Mako U130B CMOS camera-equipped optical calibration platform, we observe how the micro urine analysis device moves and see if the locations of the detection spots (ROI) on each test strip vary or not, as illustrated in Figures 3. As a driver, the system uses a 28BYJ-48 stepper motor and the specification is depicted in **Table-S3**. Although stepper motors do not accumulate errors between steps [94], it is still necessary to consider the stopping accuracy of the open loop system. As a result, each item's length must be corrected manually. Table 2 provides the measured and corrected lengths of the ten test strips.

3.4. Measurement System Stability Verification

Dark and Standard White Spectrum

Dark and standard white spectrum are essential for ensuring the efficacy and reliability of spectroscopic measurement. The dark spectrum, as shown in Figure 4(a), representing the response of the system in the absence of light, is critical for identifying any intrinsic electronic noise or stray light interference. The standard white spectrum, as shown in Figure 4(b), serves as a baseline for calibrating the measurement system. This baseline is crucial, as it shows the reflectance characteristics of the light source across various wavelengths when radiated on a standard white target. Ideally, standard white spectrum should exhibit uniform reflectance across the visible range (i.e., 400 nm to 700 nm), indicating a well-balanced light source and properly calibrated sensor. However, the observed spectrum shows significant peaks around 400 nm and just below 600 nm, with a notable decline beyond 700 nm, suggesting that the light source unevenly emits energy across these wavelengths. This irregularity implies potential issues with calibration, light source stability and sensor sensitivity, which in turn affect measurements requiring consistent sensitivity. To overcome issues like this, calibration process might be necessary to ensure accurate spectral analysis and reliable results in laboratory settings. Regular check and use of dark and standard white reflection spectra provides a comprehensive approach to system calibration, setting a precise baseline and noise level against which all samples are measured. Moreover, adjustments are made to account for ambient light intensity, which could affect the measurements. To ensure stability and consistency, a 60-second waiting period is implemented after turning on the light source before any measurements are taken. This stabilization time allows the device to adjust to any environmental light changes and ensure accurate and repeatable readings. This methodological rigor is crucial for reducing potential errors in

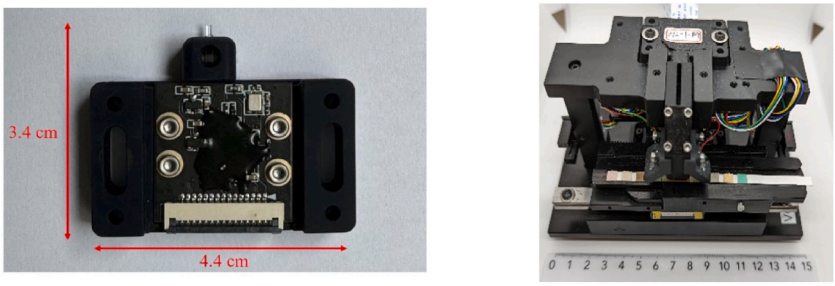

Figure 2. Micro Urine Analysis Device: (a) Spectrochip Module; (b) Assembled

Table 1
Micro Spectral Chip parameter specifications.

Parameters	Specification
Spectral Resolution	5 nm
Spectral Range	340 - 1000 nm
Spectral Accuracy	± 0.5 nm
Image Sensor	CMOS Image Sensor
Dimensions	44 × 34× 8.7 mm
Driver	28BYJ-48 stepper motor

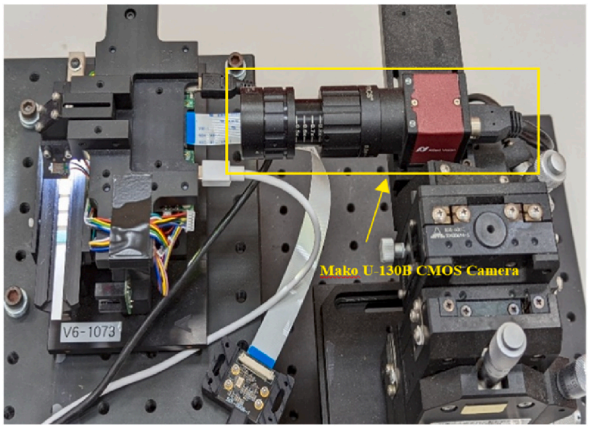

Figure 3. Observation of Test Strip Positions on the Optical Inspection Platform

Table 2
Position measurements of urine test strips in the optical inspection platform.

No.	Test Items	Measurement Length (mm)	Calibration Length (mm)	Error (mm)
Ten-parameter Urine Test Strips				
1	Leukocytes	105.31	107.30	-1.99
2	Nitrite	97.18	99.25	-2.07
3	Urobilinogen	88.73	90.95	-2.22
4	Protein	82.20	83.40	-1.20
5	pH	73.52	75.57	-2.05
6	Occult Blood	66.09	68.10	-2.01
7	Specific Gravity	59.08	60.65	-1.57
8	Ketone	50.94	52.25	-1.31
9	Bilirubin	44.35	45.65	-1.30
10	Glucose	36.00	37.20	-1.20
11	Standard White	28.00	N/A	N/A
Microalbumin Urine Test Strips				
12	Microalbumin	102.99	104.00	-1.01
13	Creatinine	94.95	95.62	0.67

biomedical analysis and enhancing the reliability of diagnostic results derived from the spectrochip system.

Instrument Stability Analysis

Prior to the stability analysis of the spectrochip, dark and standard white spectra are employed for baseline correction, and to assess the light source stability and sensor sensitivity, as shown in Figure 4. The dark spectrum plays a vital role in calibration by provides a baseline noise level (i.e., zero-point) that must be subtracted from the sample and reference spectra to correct system noise or ambient light interference, thus ensuring measurement accuracy. Additionally, the reference spectrum is essential for calibration, and ensuring accurate and reliable spectral analysis. In this study, recordings of the reference, sample, and dark spectra were taken before performing stability analysis to enhance the accuracy and consistency of the measurement system. In this spectroscopic analysis, a reference spectrum is obtained from a known standard sample with well-defined spectral characteristics. It is used as a baseline (i.e., standard) to calibrate the spectroscopy system and to compare against the spectra obtained from unknown samples, which eliminates system variations and enhances the spectral analysis accuracy [95], [96], [97].

On the other hand, the sample spectrum is the actual spectral data collected from the test sample. This spectrum displays how the

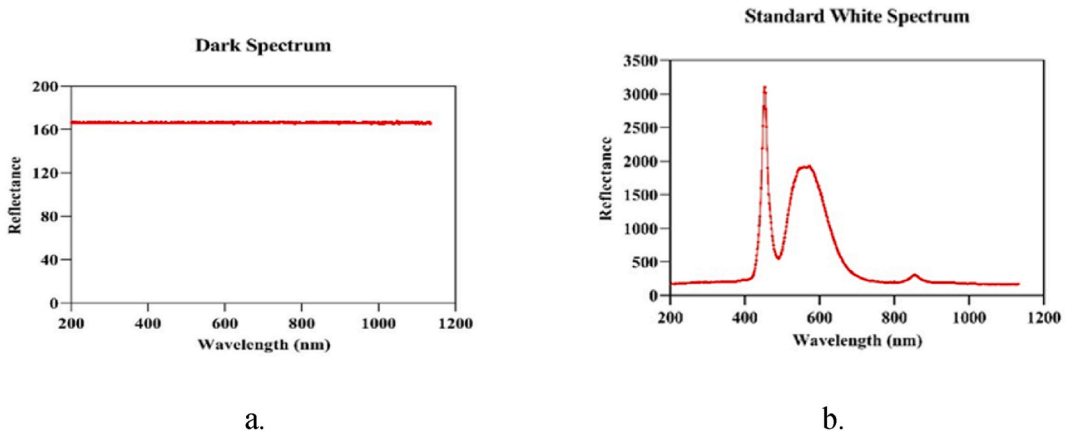

Figure 4. Reflectance spectrum: (a). Dark Spectrum, (b). Standard White Spectrum using Cree XLamp XT-E White light source.

sample interact with the light across various wavelengths. Analyzing the sample spectrum allows researchers to identify and quantify the chemical or physical characteristics of the sample based on its unique spectral signature. Finally, dry urine test strip was placed on the calibrated measurement platform and three repeated independent spectrum readings were captured. The three sets of measured spectra and the dark spectrum of the ROI subtracted from each measurement were then superimposed to ensure consistency and identify any spectral drift in the measurement system, as depicted in Figure 5. Moreover, sequential measurements on multiple test strips with varying reaction times can significantly affect the consistency of detection results. Variations in reaction times can lead to differences in the development of color changes or chemical reactions on the test strips, which may result in inconsistent readings. In this study, to ensure uniformity and reliability in the measurement results, we standardized reaction times across all tests, maintained consistent environmental conditions and strictly adhered to the prescribed testing and reading time specified for each test strip by manufacturer, as presented in Fig. S1. and Table S2. In Figure 5, the measurement results clearly illustrated that the overlaid reflectance spectra of the test strip parameters on the micro urine analyzer was within an acceptable error range.

Additionally, standard deviation (SD) and relative standard deviation (RSD) were employed to assess the variability of repeated independent measurements. SD is a basic statistical analyzing tool that quantifies the amount of dispersion of a set of data values from their mean. It provides an absolute measure of spread in the same units as the data, which is essential for identifying the extent of variability at different wavelengths for various biomarkers, as depicted in Figure 6(a). At specific wavelength, SD is calculated as the square root of the mean square deviation of repeated independent measurement from their mean value, see **equation (2)**. The higher the SD value, the greater inconsistency in the measurement readings at that wavelength. RSD, known as coefficient of variation (CV), measures the variability relative to the mean of the dataset, which facilitates comparison across different scales and concentrations by normalizing the variability, as shown in **equation (3)**.

SD can be expressed as:

$$\sigma = \sqrt{\frac{1}{N}\sum_{i=1}^{N}(x_i - \mu)^2} \tag{2}$$

where, σ is standard deviation, μ is mean of the dataset and N is total number of independent spectral measurement.

Whereas, relative standard deviation (RSD) can be expressed as:

$$RSD = \left(\frac{\sigma}{\mu}\right) \times 100\% \tag{3}$$

Figure 6(b), provides a normalized measure of variability relative to the mean intensity at each wavelength, allowing for comparison across biomarkers regardless of their concentration or intensity levels. By using SD, we can pinpoint where the greatest variations occur, while RSD offers insights into the precision and reliability of the spectrochip and highlights its performance consistency across different conditions and level of wavelength. As the result, most biomarkers show lower variability at higher wavelengths, suggesting that the spectrochip provides more stable and reliable readings in this range. Moreover, lower RSD values across the spectrum indicate high precision and reliability of the spectrochip, making it suitable for clinical applications where consistent and accurate measurements are crucial.

Test-Strip Stability Analysis

Because urine test strips are intrinsically unstable in terms of humidity and temperature after being opened [98], [99], the stability test of experimental test strips should be performed soon after the measuring instrument stability verification. BIO-RAD qUAntify Plus Control Levels-1 and Levels-2 were employed for auxiliary testing in this investigation, as shown in Figure 9. Using a mechanical micropipette, 20μl standard solution of each level is pipetted onto the test strip. For verifying the stability of urine test strips, the same

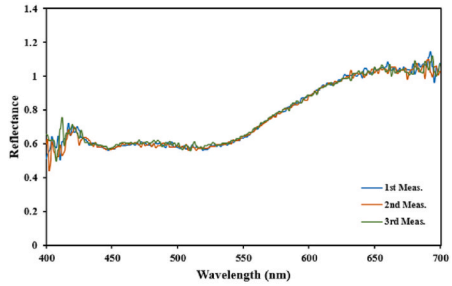

a. Leukocytes

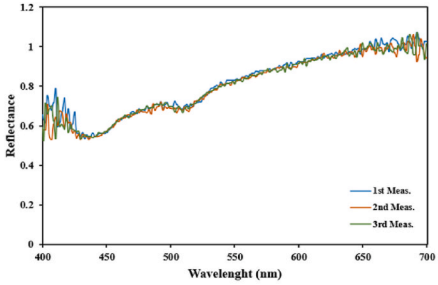

b. Nitrite

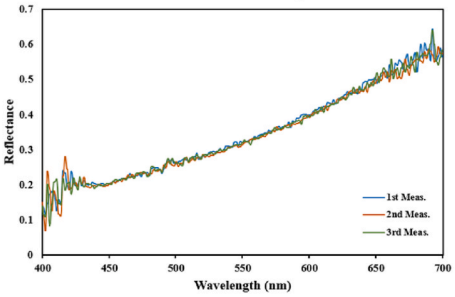

c. Urobilinogen

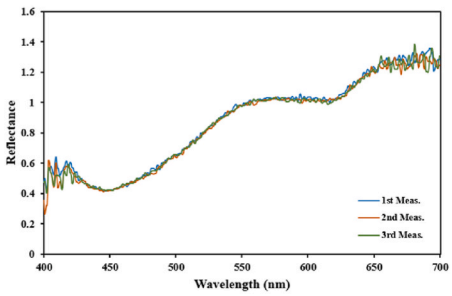

d. Protein

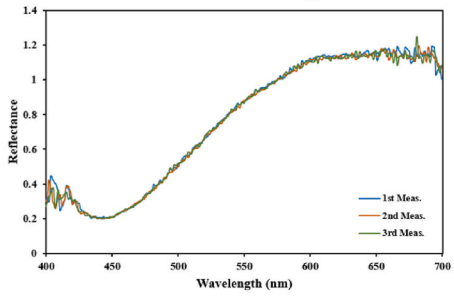

e. pH

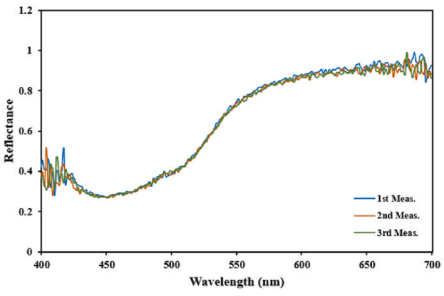

f. Occult Blood

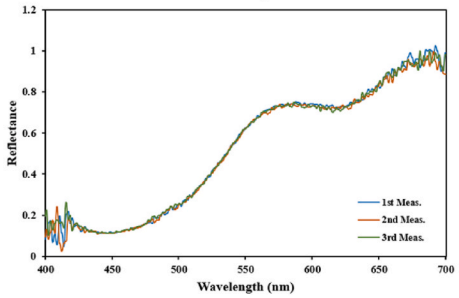

g. Specific Gravity

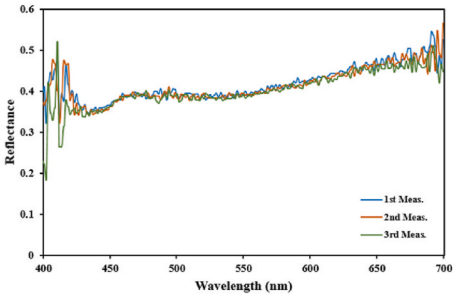

h. Ketone

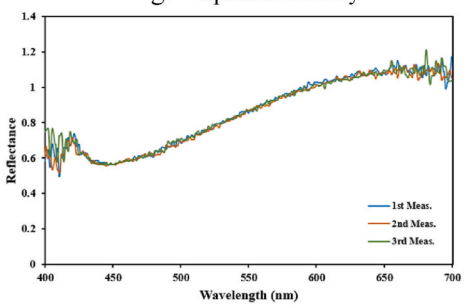

i. Bilirubin

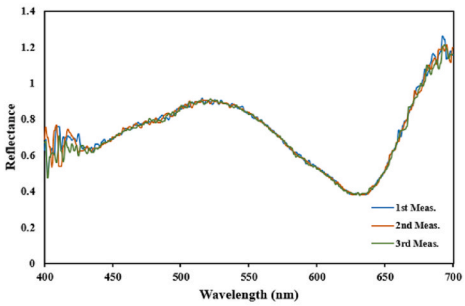

j. Glucose

(caption on next page)

Figure 5. Reflectance spectra of urine test strip ten-parameter for instrument stability verification.

procedure as previous instrument stability verification was applied to four distinct urine parameters, namely leukocytes, nitrite, protein, and ketone. For every measured parameter of the urine test strip on micro urine analyzer, the stacked spectra of the reflecting light intensity at two distinct levels of selected biomarkers, including Leukocytes, Nitrite, Protein, and Ketone, fall within the allowable error range, as displayed in Figures 7. In Figure 8, the variability of test strips is analyzed through the presentation of SD and RSD across different wavelengths for selected biomarkers. Figure 8(a) and 8(c) illustrate the SD at two distinct levels (i.e., Lv.1 and Lv.2), quantifying the spread data around the mean and thus assessing the precision of the test strips. Figure 8(b) and 8(d) depict the RSD, which normalizes the SD relative to the mean, providing a percentage-based comparison of variability across tests. The stability of SD and RSD within acceptable error ranges across both levels underscores the reliability of the test strips under diverse conditions, a critical factor for their application in precise diagnostic settings.

For further stability analysis, the Magenta Test Strip is used to evaluate the performance and consistency of the micro-spectral chip, which is mostly used to simulate the spectral properties of Nano-gold particles (AuNPs) in serum [100]. Detailed results and comprehensive analysis are available in the supplementary information, where extensive data and discussions are provided. As shown in Fig. S2., the Magenta Test Strip analysis using two LED light sources, labeled as A-light and B-light, ensures that the spectrochip can provide reliable and repeatable results, crucial for accurate diagnostics and making it well-suited for practical applications where diverse concentration levels must be accurately measured. Moreover, as mentioned in the previous section, ideal standard white spectrum should exhibit uniform reflectance. This was confirmed by magenta test strip analysis, particularly Fig. S2(d), where 5% magenta performance closely approximates white area, and ensures that the instrument was properly calibrated.

4. Result and Discussion

In this section, we explore how the absorption spectra of test samples vary with concentration. To facilitate the analysis, stable light source is selected, and its wavelength is utilized to calculate the absorbance spectra at various concentrations, which forms the basis of a Calibration Curve. This model enables the determination of unknown sample concentrations by placing them under a spectrometer with controlled external conditions. The concentration of the unknown sample is then identified by mapping its absorption intensity at the characteristic wavelength (λ_c) onto the calibration curve. This method underscores the critical role of precise calibration in achieving reliable and reproducible diagnostic results.

4.1. Standard Solution Concentration

Multiplicative dilution, often known as serial dilution, is the technique of gradually dissolving a sample in a solution using the same sample-to-solvent ratio each time, which can result in a geometric dilution of concentration. In this experiment, volumetric concentration percentage formula to perform multiplicative dilution is used, as shown in **equation (4)**. In the standard solution dilution, Bio Rad qUAntify Plus Control Level-1 used as the solvent and Level-2 as the solute. To increase the accuracy of the calibration curve, 75% is used as a variable indicator between 100% and 50%. Table 3 shows the solute-solvent ratios at different concentration levels of the solution. Figure 9 demonstrates the dilution and spectroscopic analysis of the standard solution using various tools. These tools include sterilized micro-tubes for handling the solution, a vortex mixer for uniform mixing, a micropipette for applying a 20 μl drop of the solution onto the test strip, and a test strip slot for positioning under the optical observation platform.

$$Vol\,\% = \frac{Solute\ (\mu)}{Solution\ (\mu l)} \times 100\% = \frac{Solute\ (\mu l)}{Solute\ (\mu l) + Solvent(\mu l)} \times 100\% \tag{4}$$

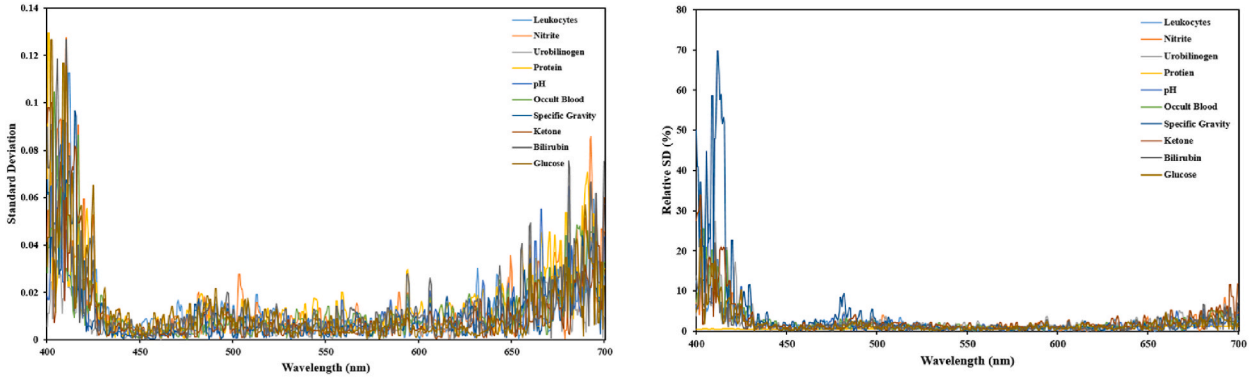

Figure 6. Instrument variability investigation: (a). SD and, (b). CV (RSD)

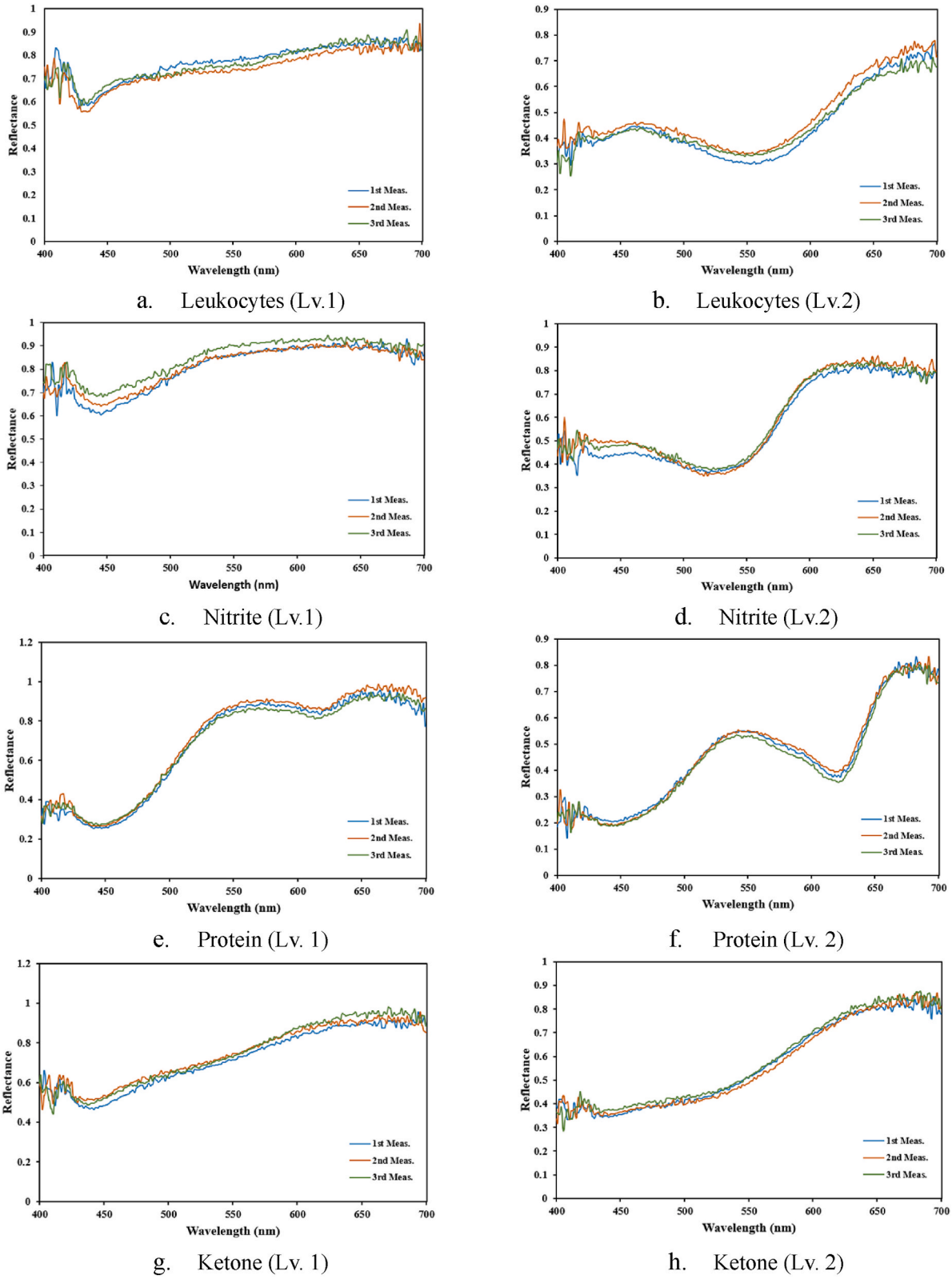

Figure 7. Reflectance spectra of four distinct urine test parameters for test strip stability verification.

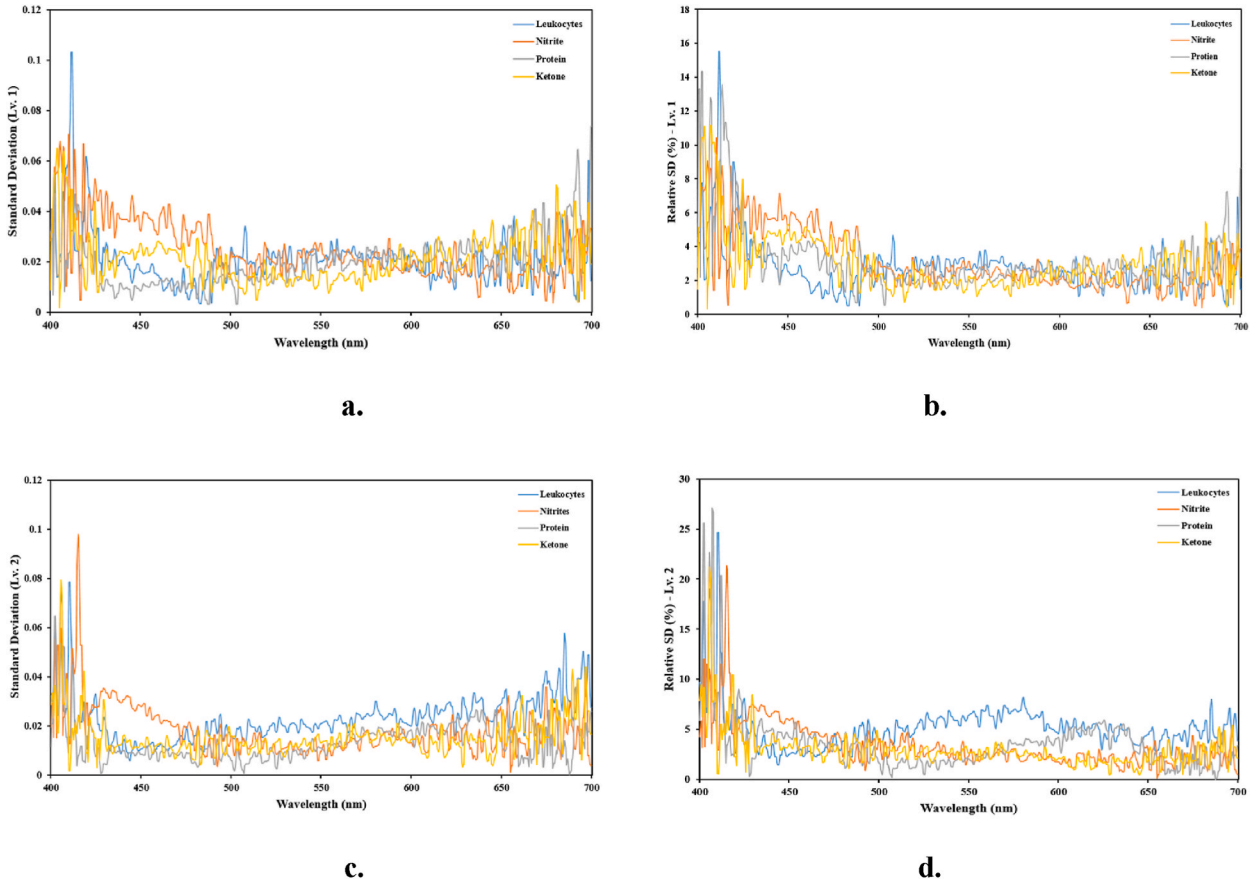

Figure 8. Test strip variability investigation: (a). SD (Lv. 1), (b). CV (RSD - Lv. 1), (c). SD (Lv. 2), and (d). CV (RSD - Lv. 2)

Then, the measurement result of standard solutions at each concentration under the micro urine analyzer is documented. The test paper is used to titrate standard solutions of each concentration, and the spectra of three repeated independent measurements are taken, as shown in Fig. S5 - Fig. S16. Figure 10 illustrates the colorimetric response of urine test strips at different analyte concentrations, providing the capacity of the test strip to visually represent changes from 0% to 100% concentration. Figure 10(a) features a ten-parameter strip, while Figure 10(b) displays a strip testing for Microalbumin with creatinine. The color gradient of each strip changes according to the analyte concentration levels, demonstrating their semi-quantitative utility for initial diagnostic screening. Moreover, this visual matrix is critical for rapid and efficient detection of various parameters in urine that are indicative of different physiological and pathological conditions.

Figure 11 (a-l) illustrates the average absorbance spectra for standard solutions of various analytes at different concentration levels, showcasing a systematic approach to determine their optical characteristics. For each analyte, ranging from Leukocytes to Creatinine, the procedure involved conducting three independent measurements at each concentration level, averaging the absorbance spectra to mitigate measurement variability, and identifying the characteristic absorption peak wavelengths. These peak wavelengths, as depicted in Table 4, are crucial for establishing calibration curves used in quantitative analysis. The spectra display how absorbance changes with concentration, providing a visual reference for the sensitivity and dynamic range of each test, which is essential for accurate calibration and subsequent analytical applications in clinical diagnostics.

Characteristic Wavelength (λ_c)

As shown in Figure 11, the average absorption spectra highlights notable absorption peaks at specific wavelength, known as characteristic wavelength (λ_c). Calibration curves are subsequently developed based on the signal intensity at these wavelengths. Table 4 presents the characteristic wavelengths for each parameter tested with urine test strips.

4.2. Calibration Curve Modelling

Regression analysis is a statistical technique used to explore the relationship between independent variables (i.e., predictors) and a dependent variable (i.e., response), aiming to create a regression equation for predicting the dependent variable. In this study, we utilized regression analysis to develop calibration curve models using GraphPad Prism, which is based on the average absorption

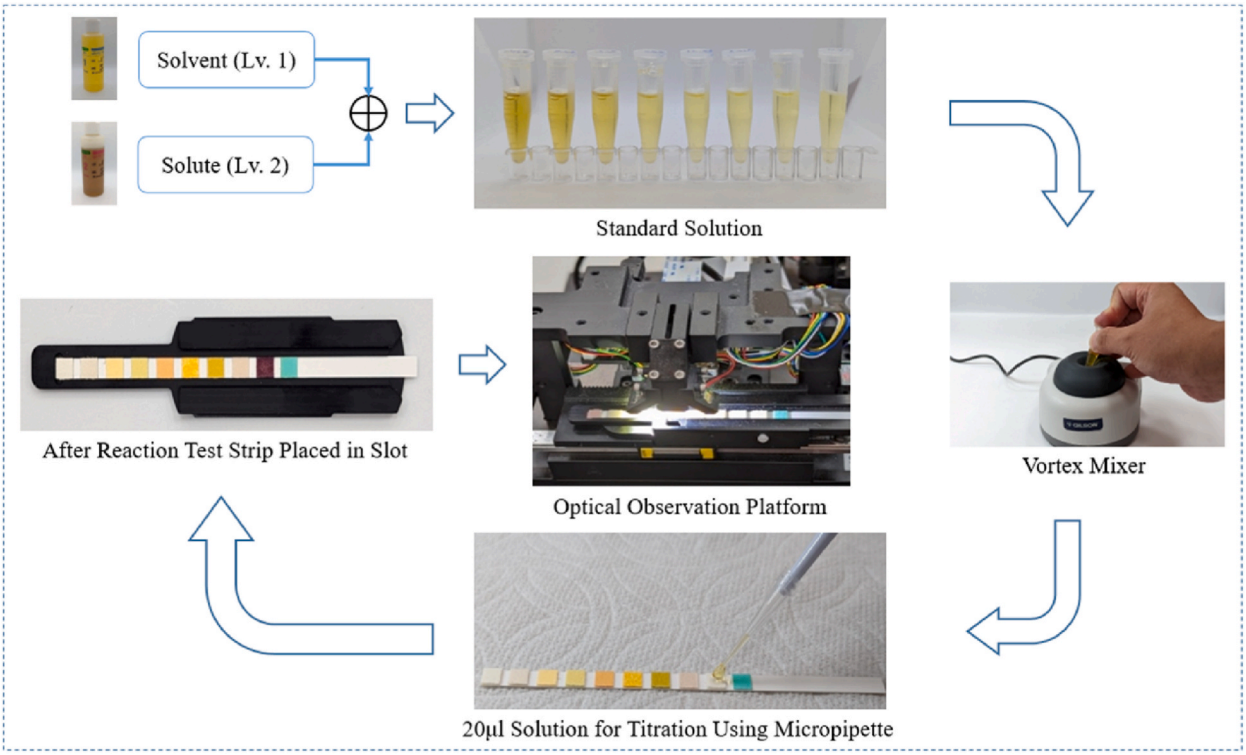

Figure 9. Spectroscopic titration procedure of diluted solution using urine test strips.

Table 3
Standard solution preparation at different solvent and solute concentration.

Concentration (%)	Level-1 (μl)	Level-2 (μl)
0%	1000	0
3.125%	968.75	31.25
6.25%	937.5	62.5
12.5%	875	125
25%	750	250
50%	500	500
75%	250	750
100%	0	1000

spectra from various concentrations. This approach helps approximate concentrations of unknown samples by inputting characteristic wavelength data into the models. Calibration curves, essential for quantifying unknown samples require at least three, or preferably five or more known concentration solutions to establish a reliable model. These curves, which plot absorbance values against concentrations may not always be linear; they are categorized into linear models (e.g., straight lines, $y = ax + b$) and nonlinear models (e.g., polynomials, logarithmic, sigmoid functions, exponential growth, and one phase association), depending on the data distribution.

Coefficient of Determination (R^2)

In statistics, coefficient of determination (R^2) indicates the extent to which the variation in the dependent variable can be explained by the independent variables. It is used to evaluate the accuracy of the model [101]. R^2 values vary from 0 to 1, with higher values indicating a stronger ability of independent variables to explain the dependent variable. Therefore, the constructed recursive model with high R^2 value is more accurate and reliable. It is expressed as:

$$R^2 = 1 - \frac{SS_{res}}{SS_{total}} \tag{5}$$

where, SS_{res} is residual sum square and SS_{total} is total sum square.

However, because of the sample size, the R^2 value can be incorrectly calculated. Overestimation is more likely to occur with smaller sample sizes. The sum of squared residuals will only go down as the number of independent variables, 'x' becomes up, increasing R^2. A greater R^2 denotes a better explanatory capacity, however it might become unstable if there are excessively many irrelevant

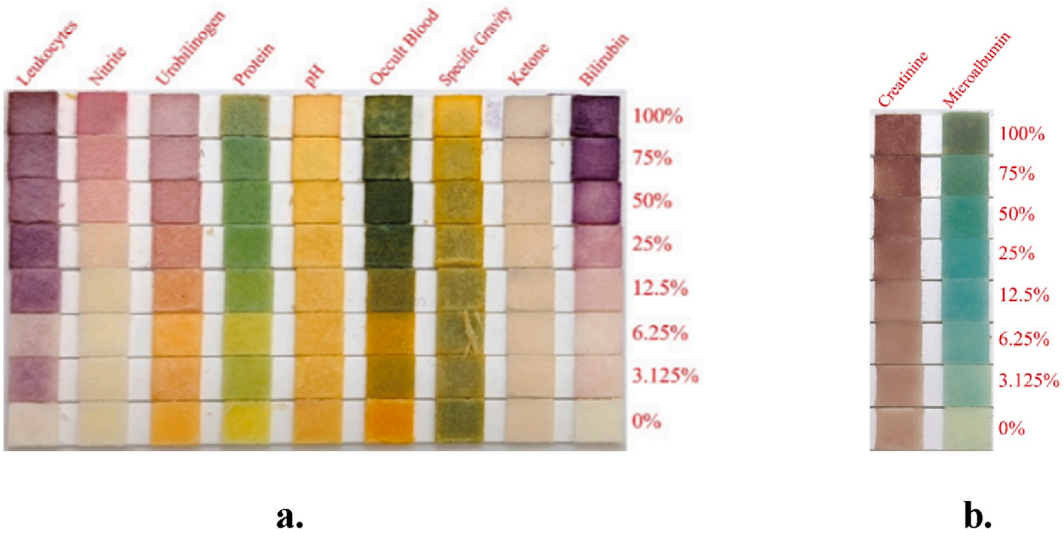

Figure 10. Pictures of urine test strips at different concentrations after the reaction: (a). Ten-parameter urine test strips, (b). Microalbumin with creatinine urine test strips.

independent variables, 'x'. Consequently, using the method in **equation (5)**, the adjusted coefficient of determination (Adjusted R^2, or $\overline{R^2}$) is obtained by accounting for the number of variables and samples, as expressed in **equation (6)** below.

$$\overline{R^2} = 1 - \frac{\frac{SS_{res}}{n-p-1}}{\frac{SS_{total}}{n-1}} \tag{6}$$

where, n is the number of samples and p is the number of variables.

Calibration Curve Model (CCM)

In this study, we developed a calibration curve model for twelve urine parameters, each adopted to the unique biochemical and physical properties of the analytes, which are critical for clinical diagnostics. These urine parameters are analyzed under controlled laboratory conditions. This model integrates both concentration levels standard solutions and average spectral signal intensities across varying characteristic wavelengths, detailed in Table S6 and Table S7 in the supportive information. For each parameter, absorption spectra were measured three times independently at eight different concentration levels (see Fig. S5 to Fig. S16, where the measurement results for each biomarker are depicted) and the average intensities were calculated to establish robust calibration curve, as depicted in Figure 11. The regression equations were obtained using GraphPad Prism analysis, as shown in Table 5. The CCM graphs are presented in Figure 12, which are a crucial element in the quantification of urine analytes. Each curve is meticulously plotted to reflect the concentration-dependent changes in signal intensity, thereby facilitating the precise determination of analytes concentration in unknown samples. The shape of the curve depends on the biochemical properties of the analyte and the characteristics of the reaction with the test strip reagents.

These curves are then used to drive regression equations, which mathematically describe the curve and can be used to calculate the concentration of the analytes in urine samples based on their measured intensities. Moreover, these equations are also critical for transforming raw spectral data into meaningful clinical information, enabling healthcare providers to perform accurate and reliable urinalysis. As depicted in Figure 12(a), Leukocytes were analyzed at 550 nm CW using a dual-model approach to accurately represent both low and high concentration levels through an exponential growth pattern, characterized by nonlinear regression equations. This bifurcated approach caters to the semi-quantitative nature of leukocyte detection in clinical settings, facilitating a more nuanced interpretation of urinary leukocyte concentrations. Nitrite analysis at 520 nm demonstrated a linear relationship between concentration and spectral signal intensity, as shown in Figure 12(b). It is ideal for detecting bacterial infections in the urinary system. The straightforward linear regression model allows for precise nitrite quantification. Urobilinogen, measured at CW of 570 nm, exhibited an exponential growth pattern in its response curve, as shown in Figure 12(c), indicative of the complex biochemical interactions of Urobilinogen in urine. This nonlinear approach is crucial for assessing liver function and detecting hemolysis.

Protein was quantified at 620 nm CW, where the calibration curve showed an exponential increase with concentration, as shown in Figure 12(d), which reflects the aggregation of protein-dye complexes on the test strips. This model is vital for the detection of proteinuria, a common symptom of kidney disease. pH values were determined at 615 nm CW, which is essential for monitoring metabolic and kidney disorders. Due to the calculation method of pH values being based on the concentration of hydrogen ions, this section includes two calibration curves, one for hydrogen ion concentration and another for direct pH value measurement.

As depicted in Figure 12(e), using an exponential decay function to accurately model the logarithmic nature of hydrogen ion concentration. Whereas, as shown if Figure 12(f), a direct pH measurement exhibits a linear pattern. Therefore, a linear equation was

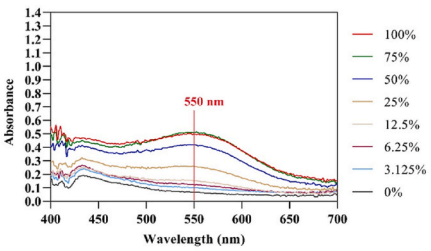

a. Leukocytes

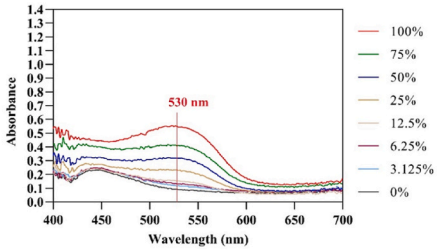

b. Nitrite

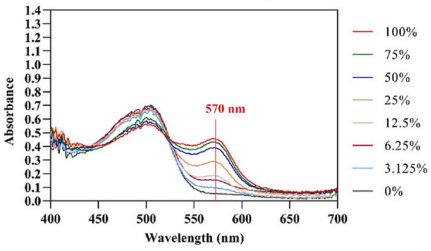

c. Urobilinogen

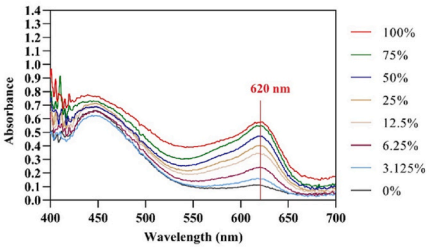

d. Protein

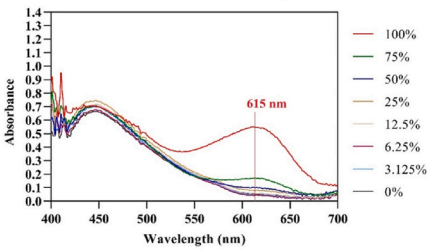

e. pH

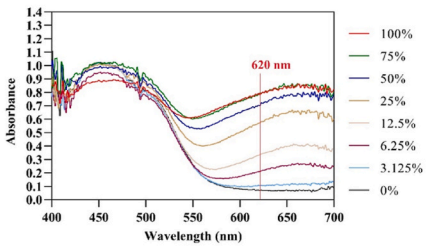

f. Occult Blood

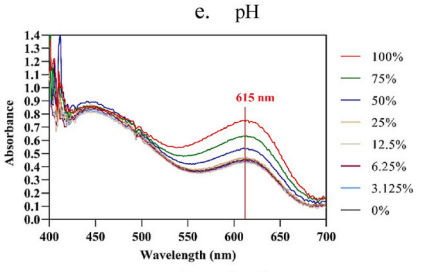

g. Specific Gravity

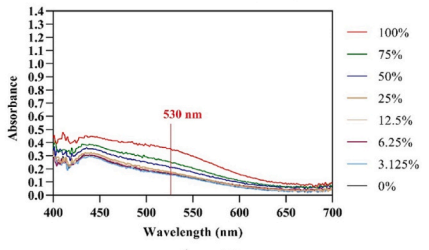

h. Ketone

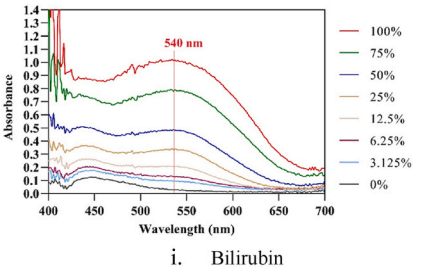

i. Bilirubin

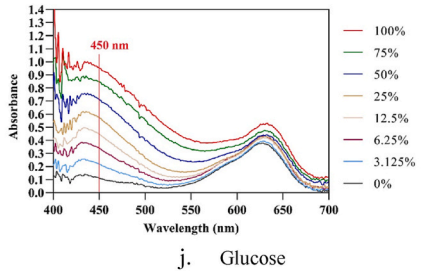

j. Glucose

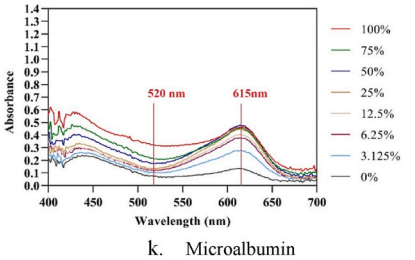

k. Microalbumin

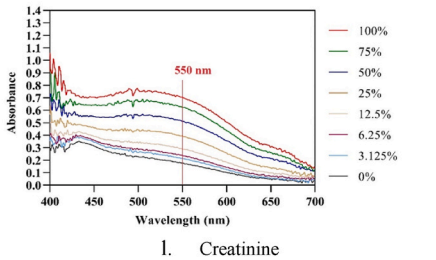

l. Creatinine

(caption on next page)

Figure 11. Average Absorbance spectra of standard solution at different concentration.

Table 4
Characteristic wavelengths of the twelve absorption peaks.

Items	Characteristic Wavelength (nm)
Leukocytes	550
Nitrite	530
Urobilinogen	570
Protein	620
pH	615
Occult Blood	620
Specific Gravity	615
Ketone	530
Bilirubin	540
Glucose	450
Microalbumin	520 & 615
Creatinine	550

Table 5
Calibration Curve Model (CCM) and Coefficient of Determination (R^2)

S.N.	PARAMETER	CCM	R^2	REMARK
1.	Leukocytes (Min. Conc.)	$y = 0.05765 + 0.53815 \cdot \left(1 - e^{-0.004118x}\right)$	0.9788	(7)
2.	Leukocytes (Max. Conc.)	$y = 0.03259 + 0.56741 \cdot \left(1 - e^{-0.004109x}\right)$	0.9760	(8)
3.	Nitrite	$y = 0.8704x + 0.1008$	0.9892	(9)
4.	Urobilinogen	$y = -0.1177 + 0.5875 \cdot \left(1 - e^{-1.802x}\right)$	0.9923	(10)
5.	Protein	$y = -0.01081 + 0.56641\left(1 - e^{-0.0259x}\right)$	0.9685	(11)
6.	pH (H^+)	$y = 0.5572 \cdot e^{-0.3476x}$	0.9564	(12)
7.	pH (Pure)	$y = 0.2550x - 1.492$	0.9931	(13)
8.	Occult Blood (Min. Conc.)	$y = 0.04136 + 0.77084 \cdot \left(1 - e^{-0.5471x}\right)$	0.9912	(14)
9.	Occult Blood (Max. Conc.)	$y = -0.04415 + 0.85635 \cdot \left(1 - e^{-0.5611x}\right)$	0.9912	(15)
10.	Specific Gravity	$y = 0.4174 + \frac{0.4891}{1 + 10^{-217.5(1.012 - x)}}$	0.9730	(16)
11.	Ketone (Min. Conc.)	$y = 0.1454 \cdot e^{0.05432x}$	0.9548	(17)
12.	Ketone (Max. Conc.)	$y = 0.09675 \cdot e^{0.08148x}$	0.9548	(18)
13.	Bilirubin	$y = 0.2425x + 0.03828$	0.9901	(19)
14.	Glucose	$y = 0.1382 + 0.81277 \cdot \left(1 - e^{-0.006123x}\right)$	0.9739	(20)
15.	Microalbumin (520nm)	$y = 0.09712 \cdot e^{0.01712x}$	0.9499	(21)
16.	Microalbumin (615nm)	$y = 0.03357 + 0.42583 \cdot \left(1 - e^{-0.2793x}\right)$	0.9756	(22)
17.	Microalbumin (520nm*615nm)	$y = 0.1756 + 0.5141 \cdot \left(1 - e^{-0.1416x}\right)$	0.9071	(23)
18.	Microalbumin (520nm*615nm, excluding 100% data)	$y = 0.1231 + 0.515 \cdot \left(1 - e^{-0.2116x}\right)$	0.9558	(24)
19.	Creatinine	$y = 0.004174x + 0.1623$	0.9744	(25)

utilized for analysis purpose. Occult Blood detection was modeled at 620 nm CW with exponential decay equations for both low and high concentration ranges, reflecting the semi-quantitative nature of occult blood testing, as illustrated in Figure 12(g). This is critical for detecting conditions ranging from infections to cancers in the urinary tract. Specific Gravity measurements at CW of 615 nm utilized a nonlinear equation to capture the subtle changes in urine concentration, which is a key indicator of kidney health, see Figure 12(h). Ketone levels, analyzed at CW of 530 nm, required separate calibration curves for low and high concentrations due to its semi-quantitative detection, important for monitoring metabolic conditions such as diabetes, as illustrated in Figure 12(i). Bilirubin was assessed at 540 nm CW with a linear model, reflecting its stable increase with concentration, which is directly related to liver function, as shown in Figure 12(j). Glucose, measured at CW of 450 nm, followed an exponential calibration curve, see Figure 12(k), which highlights the enzymatic reaction kinetics used in glucose testing, significant for diagnosing diabetes.

Microalbumin was uniquely analyzed at dual characteristic wavelengths, showing exponential growth patterns at both of 520 nm and 615 nm, see Figure 11, which are critical for detecting early stages of kidney damage. As shown in Figure 12(l) & Figure 12(m), it is observed that the distribution of the two calibration curve models is not identical. To validate the accuracy of the models, the absorption peak values at 520 nm and 615 nm were multiplied, and a new calibration curve was reconstructed. The spectral signal intensity after multiplying the values at 520 nm and 615 nm characteristic wavelength is depicted in Table S7. As illustrated in Figure 12(n), the model is more identical to Figure 12(m), which exhibits a gradual exponential growth pattern. Therefore, a nonlinear equation was employed for the Microalbumin analysis. However, in Figure 12(n), it is evident that the 100% concentration level absorption data deviates from the model range, indicating an outlier. Therefore, it is determined that the concentration level of 100% absorption data is oversaturated for Microalbumin. During the modeling process, this data was excluded to improve the accuracy of the model, and the model was reconstructed accordingly, as illustrated in Figure 12(o). Finally, Creatinine quantification at 550 nm CW

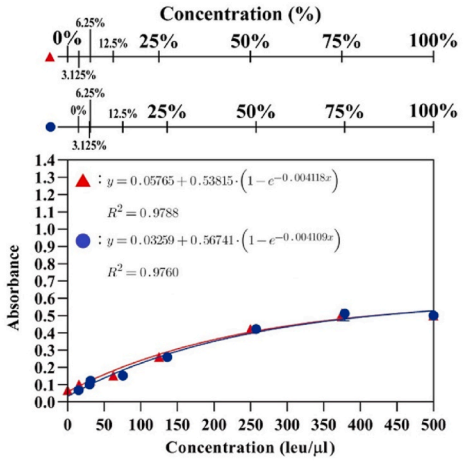

a. Leukocytes

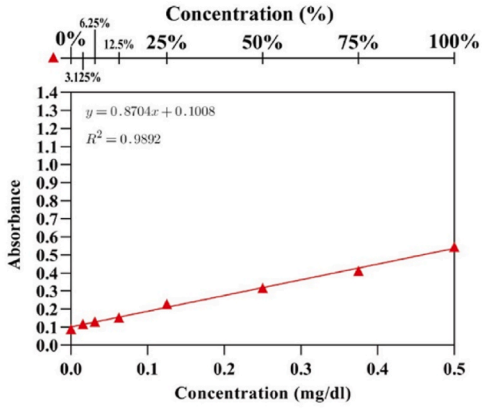

b. Nitrite

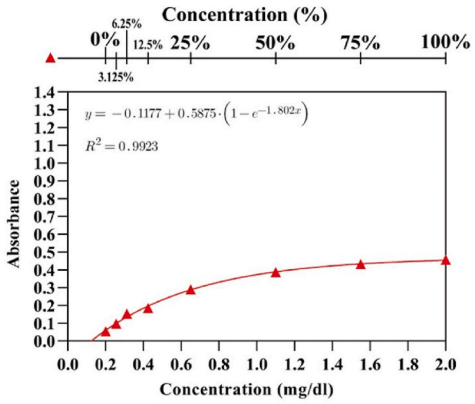

c. Urobilinogen

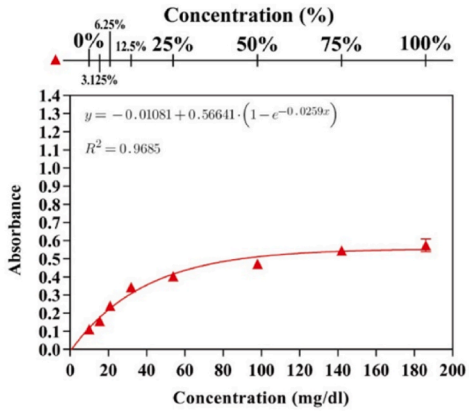

d. Protein

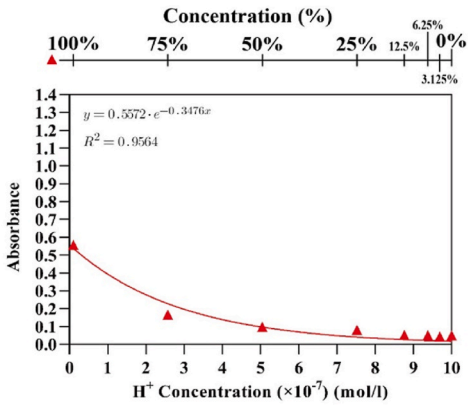

e. Hydrogen ion (H^+) concentration

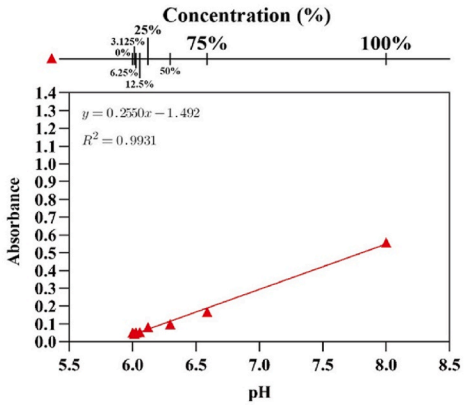

f. Direct pH values

Figure 12. Calibration curve model (CCM) of twelve urine parameters.

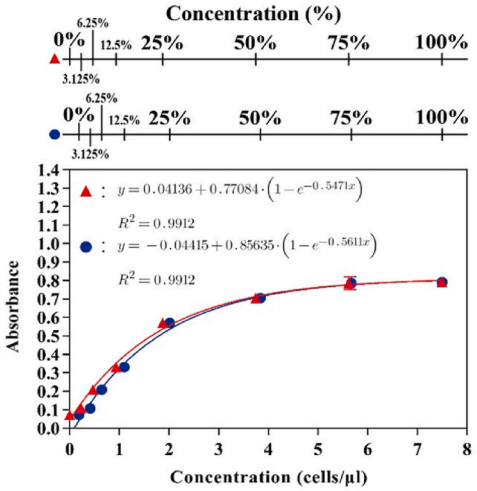

g. Occult Blood (▲: low & ●: high)

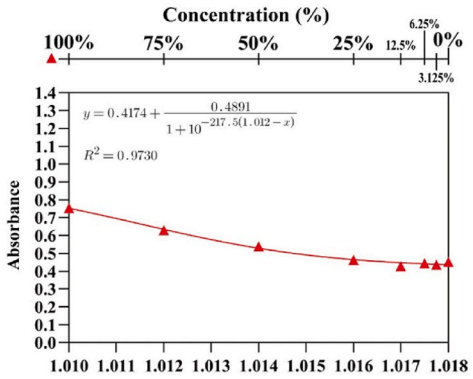

h. Specific Gravity

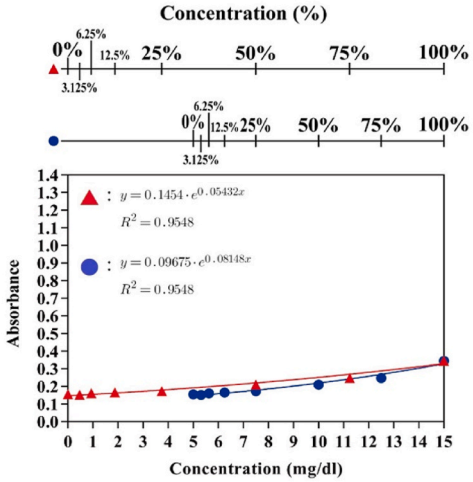

i. Ketone (▲: low & ●: high)

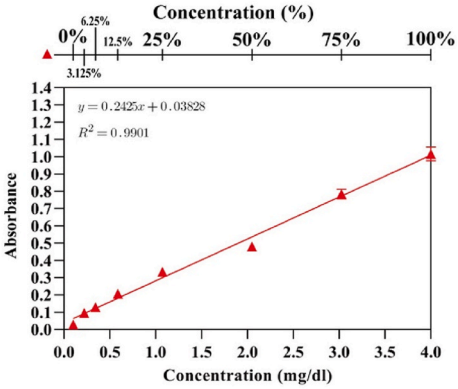

j. Bilirubin

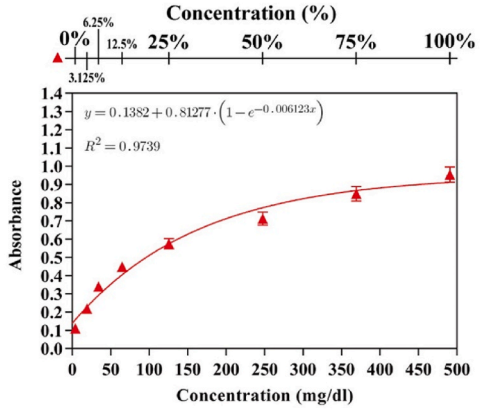

k. Glucose

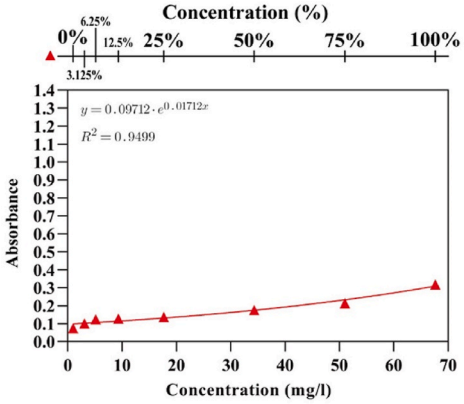

l. Microalbumin (520 nm)

Figure 12. (*continued*).

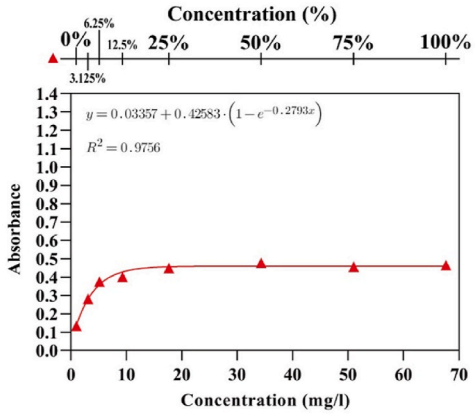

m. Microalbumin (615 nm)

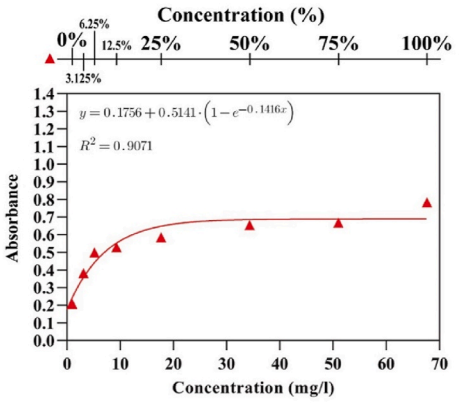

n. Microalbumin (520 nm * 615 nm)

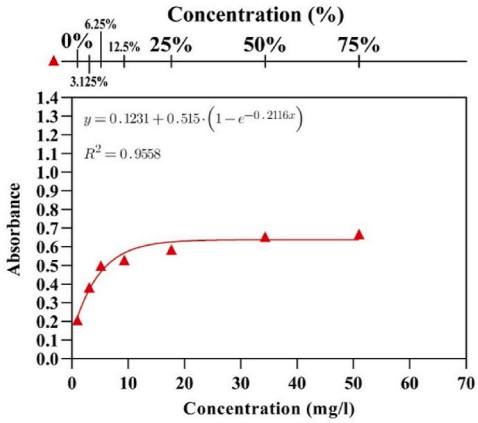

o. Modified Microalbumin (520 nm * 615 nm)

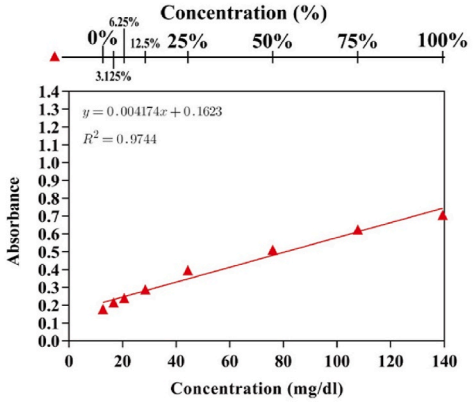

p. Creatinine

Figure 12. (*continued*).

was modeled using a linear regression, as illustrates in Figure 12(p), which provides a reliable measure of renal function crucial for the clinical assessment of kidney health. Each urine parameter's model was carefully developed to achieve optimal accuracy in our diagnostic instruments, reflecting the complexities of urinary analysis and its clinical implications. These detailed calibration curves and regression models serve as a robust foundation for reliable urinary diagnostics.

Qualitative and Quantitative Chemical Analysis

In analytical chemistry, qualitative analysis determines the presence of a substance with results typically labeled as "positive" or "negative," while quantitative analysis provides precise numerical values to specify sample composition. For cases where the presence of a substance is confirmed but full quantitative precision is unattainable due to measurement limitations, "Semi-Quantitative Analysis" is used to estimate a rough concentration range. This method is less precise but suitable for quick assessments when only approximate values are needed. In this study, to improve the accuracy of sample measurements in Level-1 and Level-2 standard solutions, the

Table 6
Quantitative analysis values for selected five semi-quantitative biomarkers.

Item	Level 1 Semi-quantitative value	Level 1 Quantitative value	Level 2 Semi-quantitative value	Level 2 Quantitative value
Protein	Negative	9.96mg/dl	2+	186.07 mg/dl
Bilirubin	Negative	0.10 mg/dl	3+	4.00 mg/dl
Glucose	Negative	4 mg/dl	2+	491 mg/dl
Microalbumin	N/A	1.00 mg/l	N/A	67.66 mg/l
Creatinine	N/A	12.70 mg/dl	N/A	139.40 mg/dl

prepared samples were analyzed in a laboratory. The detailed results are presented in Table 6, derived from data provided by the manufacturer (refer to Fig. S1 & Table S2) and analyzed using SIEMENS CLINITEK Novus Automated Urine Chemistry Analyzer (see Fig. S3). Five selected semi-quantitative urine parameters, namely protein, bilirubin, glucose, microalbumin, and creatinine, were analyzed to illustrate the precision in quantitative analysis performance of micro urine analyzer, and the measurement data are presented in Table 6. The rough comparison of micro-urine analyzer with SIEMENS CLINITEK Novus Automated Urine Chemistry Analyzer are presented in Table S4 of the supporting information.

4.3. Trade-offs: Benefits and Challenges of Proposed Protocol

The introduction of the spectrochip-based measurement system represents a significant step forward in urinalysis, offering a blend of accuracy, portability, and efficiency that is not typically found in conventional protocols. This measurement system utilizes MEMS-based technology to minimize footprint of large-scale diagnostic equipment, significantly enhancing point-of-care (POC) testing capabilities. Achieving an R^2 over 0.95, the system provides reliable diagnostic outcomes, equating its performance with that of larger, established instruments and mitigating concerns about the accuracy and reliability of smaller-scale diagnostics. Its compact design facilitates use in diverse environments, including remote areas, and reduces operational costs significantly. The built-in environmental shielding addresses the challenge of ambient light sensitivity (see Fig. S4), enabling consistent performance outside traditional lab settings. Additionally, the use of a white LED light source reduces power consumption, increasing the lifespan of the instrument and making it suitable for areas with limited power resources.

However, the proposed method requires initial calibration using samples with known concentrations to build accurate calibration curves, a time-consuming process that necessitates access to standard solutions. Moreover, the open-loop system design necessitates manual calibration and adjustments based on the results or changing conditions to maintain precise stopping accuracy in the optical observation platform, highlighting an area for potential improvement. To address these challenges, future developments could include integrating a closed-loop control for real-time feedback adjustments, minimizing human error and improving reliability. Additionally, incorporating automated data analysis and machine learning algorithms could refine the accuracy and usability of the system by automatically correcting deviations in real-time, based on accumulated data trends, thereby improving both the user experience and the accuracy of the results. Ultimately, the spectrochip-based system demonstrates considerable potential to revolutionize urinalysis, aligning with the need for technically adept, cost-effective, and adaptable healthcare solutions. Future research should aim to further enhance its robustness and integrate advanced computational technologies to expand its clinical and field applications.

5. Conclusion

In this study, spectrochip-based urine analyzer was used to ensure POC testing for early detection and targeted care of potential urinary system abnormalities. To reduce power consumption, size, and increase lifespan of the instrument a white LED was selected as the light source. Experimental results on measurement system stability check illustrated that the measurements of the twelve urine test parameters at various concentrations do not exhibit significant fluctuations, and its SD and RSD (CV) fell within acceptable ranges. For each parameter of urine test strips, absorption spectra were measured three times independently at eight different concentrations (i.e., 100%, 75%, 50%, 12.5%, 6.25%, 3.125%, and 0%) of a standard solution, and the average spectral intensities were calculated to establish the calibration curve under the characteristic wavelength (λ_c) of the maximum absorption peaks. Next, utilizing GraphPad Prism, regression analysis was performed on the modeled calibration curve to determine the coefficient of determination (R^2) for each parameter. As confirmed by the result, the values of R^2 being over 0.95, the routine urine analysis using micro-spectrometer is both accurate and reliable. In future comparisons with calibration curves, even when sample concentration is unknown, it is possible to obtain the spectral signal at characteristic wavelength of each parameter. Additionally, the spectrochip-based measurement system simplifies the complex and time-consuming design of large commercial instruments due to its compact size, portability, and accuracy. It is easily affordable for the general public and is not restricted by the location of medical laboratories. It can also efficiently prevent diseases and minimize healthcare costs. In general, the proposed micro-spectrometer measurement system offers a portable, cost-effective, and efficient solution for point-of-care testing, despite some challenges related to initial calibration, manual correction and environmental sensitivity. Future enhancements could integrate closed-loop control and automated data analysis with machine learning algorithms to provide real-time feedback and automatic corrections, improving accuracy, reliability, and user experience.

Data availability

-Data will be made available on request.

Ashenafi Belihu Tadesse: Writing – review & editing, Writing – original draft, Visualization, Validation, Software, Methodology, Formal analysis, Data curation, Conceptualization. Cheng-Hao Ko: Visualization, Validation, Supervision, Project administration, Methodology, Investigation, Funding acquisition, Data curation, Conceptualization. Abel Chernet Kabiso: Writing – review & editing, Writing – original draft, Visualization, Software, Methodology, Formal analysis, Data curation, Conceptualization

Declaration of Competing Interest

The authors declare that they have no known competing financial interests or personal relationships that could have appeared to

influence the work reported in this paper.

Appendix A. Supplementary data

Supplementary data to this article can be found online at https://doi.org/10.1016/j.heliyon.2024.e37722.

References

[1] A. C.Guyton andJ. E.Hall, Testbook of Medical Physiology, 11th ed. SAUNDERS ELSEVIER, 2011.
[2] B. S.Abdulwahed, A.Al-Naji, andI.Al-Rayahi, "Urine color analysis based on a computer vision system: A review," in AIP Conference Proceedings, 2023. doi: 10.1063/5.0154589.
[3] M. Nielsen, A. Qaseem, Hematuria as a marker of occult urinary tract cancer: Advice for high-value care from the American college of physicians, Ann. Intern. Med. 164 (7) (2016) 488–497, https://doi.org/10.7326/M15-1496.
[4] J.M. Sauret, G. Marinides, G.K. Wang, Rhabdomyolysis, Am. Fam. Physician 65 (5) (2002) 907–912, https://doi.org/10.1007/978-3-319-19668-8_47.
[5] L.O. Chavez, M. Leon, S. Einav, J. Varon, Beyond muscle destruction: A systematic review of rhabdomyolysis for clinical practice, Crit. Care 20 (1) (2016), https://doi.org/10.1186/s13054-016-1314-5.
[6] C. Cavanaugh, M.A. Perazella, Urine Sediment Examination in the Diagnosis and Management of Kidney Disease: Core Curriculum 2019, Am. J. Kidney Dis. 73 (2) (2019) 258–272, https://doi.org/10.1053/j.ajkd.2018.07.012.
[7] A.K. Yetisen, M.S. Akram, C.R. Lowe, Paper-based microfluidic point-of-care diagnostic devices, Lab Chip 13 (12) (2013) 2210–2251, https://doi.org/10.1039/c3lc50169h.
[8] E. R.Kandel, J. H.Schwartz, T. M.Jessell, S.Siegelbaum, A. J.Hudspeth, andS. (Eds.).Mack, *Principles of Neural Science*. New York: McGraw-Hill, 2000.
[9] D.Harvey, Modern Analytical Chemistry, 1st ed., vol. 475. McGraw-Hill, 2000. doi: 10.17660/actahortic.1998.475.58.
[10] F.Rouessac andA.Rouessac, Chemical Analysis: Modern Instrumentation Methods and Techniques, 2nd ed., vol. 11, no. 4. West Sussex: John Wiley & Sons, Ltd, 2007. doi: 10.1080/00032717808067868.
[11] A.O. Ogunfowokan, A.S. Adekunle, B.A. Oyebode, J.A.O. Oyekunle, A.O. Komolafe, G.O. Omoniyi-Esan, Determination of Heavy Metals in Urine of Patients and Tissue of Corpses by Atomic Absorption Spectroscopy, Chem. Africa 2 (4) (2019) 699–712, https://doi.org/10.1007/s42250-019-00073-y.
[12] S. Svane, H. Karring, A comparison of the transition metal concentrations in the faeces, urine, and manure slurry from different livestock animals related to environmentally relevant microbial processes, Cogent Chem. 5 (1) (2019) 1644702, https://doi.org/10.1080/23312009.2019.1644702.
[13] P.L. Jooste, E. Strydom, Methods for determination of iodine in urine and salt, Best Pract. Res. Clin. Endocrinol. Metab. 24 (1) (2010) 77–88, https://doi.org/10.1016/j.beem.2009.08.006.
[14] C. R.Li, C. C.Yang, H. Y.Tsai, C. H.Chou, K. C.Huang, andY. H.Lin, "Quantifying the glucose concentration in urine test strip with a color-calibrated imaging system," 2021 IEEE Sensors Appl. Symp. SAS 2021 - Proc., pp. 1–6, 2021, doi: 10.1109/SAS51076.2021.9530141.
[15] J. Pang, Y. Huang, Y. Liu, W. Huang, Applications of ion chromatography in urine analysis: A review, J. Chromatogr. A 1706 (June) (2023) 464231, https://doi.org/10.1016/j.chroma.2023.464231.
[16] M. Bastawrous, A. Jenne, M. Tabatabaei Anaraki, A.J. Simpson, In-vivo NMR spectroscopy: A powerful and complimentary tool for understanding environmental toxicity, Metabolites 8 (2) (2018) 1–24, https://doi.org/10.3390/metabo8020035.
[17] G.G. Harrigan, et al., Application of high-throughput Fourier-transform infrared spectroscopy in toxicology studies: Contribution to a study on the development of an animal model for idiosyncratic toxicity, Toxicol. Lett. 146 (3) (2004) 197–205, https://doi.org/10.1016/j.toxlet.2003.09.011.
[18] I. Notingher, et al., Discrimination between ricin and sulphur mustard toxicity in vitro using Raman spectroscopy, J. R. Soc. Interface 1 (1) (2004) 79–90, https://doi.org/10.1098/rsif.2004.0008.
[19] S.A. Ahmed, et al., Combating Essential Metal Toxicity: Key Information from Optical Spectroscopy, ACS Omega 5 (25) (2020) 15666–15672, https://doi.org/10.1021/acsomega.0c01898.
[20] B.G. Osborne, Near-Infrared Spectroscopy in Food Analysis, Encycl. Anal. Chem. Appl. theory Instrum. (2006) 1–14, https://doi.org/10.1002/9780470027318.a1018.
[21] D. Yang, Y. Ying, Applications of raman spectroscopy in agricultural products and food analysis: A review, Appl. Spectrosc. Rev. 46 (7) (2011) 539–560, https://doi.org/10.1080/05704928.2011.593216.
[22] D. W.Sun, Ed., Infrared Spectroscopy for Food Quality Analysis and Control. Dublin: Acadamic Press, 2009.
[23] M. Kharbach, M. Alaoui Mansouri, M. Taabouz, H. Yu, Current Application of Advancing Spectroscopy Techniques in Food Analysis: Data Handling with Chemometric Approaches, Foods 12 (14) (2023) 1–46, https://doi.org/10.3390/foods12142753.
[24] M. Jamrógiewicz, Application of the near-infrared spectroscopy in the pharmaceutical technology, J. Pharm. Biomed. Anal. 66 (2012) 1–10, https://doi.org/10.1016/j.jpba.2012.03.009.
[25] M.I. Oshtrakh, V.A. Semionkin, Mössbauer spectroscopy with a high velocity resolution: Advances in biomedical, pharmaceutical, cosmochemical and nanotechnological research, Spectrochim. Acta - Part A Mol. Biomol. Spectrosc. 100 (2013) 78–87, https://doi.org/10.1016/j.saa.2012.03.020.
[26] J. Aaltonen, K.C. Gordon, C.J. Strachan, T. Rades, Perspectives in the use of spectroscopy to characterise pharmaceutical solids, Int. J. Pharm. 364 (2) (2008) 159–169, https://doi.org/10.1016/j.ijpharm.2008.04.043.
[27] R.T. Berendt, D.M. Sperger, E.J. Munson, P.K. Isbester, Solid-state NMR spectroscopy in pharmaceutical research and analysis, TrAC - Trends Anal. Chem. 25 (10) (2006) 977–984, https://doi.org/10.1016/j.trac.2006.07.006.
[28] K. Ali, A.R.M. Albakaa, Z.H.A. Ali, New assay method UV spectroscopy for determination of Indomethacin in pharmaceutical formulation, J. Chem. Pharm. Res. 7 (4) (2015) 1591–1596 [Online]. Available: https://www.researchgate.net/profile/Ali-Albakaa-3/publication/301634930_New_assay_method_UV_spectroscopy_for_determination_of_indomethacin_in_pharmaceutical_formulation/links/5d86557392851ceb792b0a48/New-assay-method-UV-spectroscopy-for-determination-of-.
[29] W.H. Chiu, et al., A Faster, Novel Technique to Detect COVID-19 Neutralizing Antibodies, Med. Sci. Monit. 28 (2022) 1–9, https://doi.org/10.12659/MSM.935812.
[30] J. Ma, F. Meng, Y. Zhou, Y. Wang, P. Shi, Distributed water pollution source localization with mobile UV-visible spectrometer probes in wireless sensor networks, Sensors (Switzerland) 18 (606) (2018) 1–19, https://doi.org/10.3390/s18020606, 2.
[31] Y. Hu, Y. Wen, X. Wang, Detection of water quality multi-parameters in seawater based on UV-Vis spectrometry, Ocean. 2016 - Shanghai (2016) 1–4, https://doi.org/10.1109/OCEANSAP.2016.7485737.
[32] A. Avagyan, B.R.K. Runkle, L. Kutzbach, Application of high-resolution spectral absorbance measurements to determine dissolved organic carbon concentration in remote areas, J. Hydrol. 517 (2014) 435–446, https://doi.org/10.1016/j.jhydrol.2014.05.060.
[33] J. Van DenBroeke, G. Langergraber, A. Weingartner, On-line and in-situ UV/vis spectroscopy for multi-parameter measurements: a brief review, Spectrosc. Eur. 18 (4) (2006) 4–7.
[34] X. Chen, et al., Turbidity compensation method based on Mie scattering theory for water chemical oxygen demand determination by UV-Vis spectrometry, Anal. Bioanal. Chem. 413 (3) (2021) 877–883, https://doi.org/10.1007/s00216-020-03042-4.

[35] H. Zhang, L. Zhang, S. Wang, L.S. Zhang, Online water quality monitoring based on UV–Vis spectrometry and artificial neural networks in a river confluence near Sherfield-on-Loddon, Environ. Monit. Assess. 194 (9) (2022) 630, https://doi.org/10.1007/s10661-022-10118-4.
[36] P. Massey, M.M. Hanson, Astronomical spectroscopy, Planets, Stars Stellar Syst. 2 (2010) 35–98, https://doi.org/10.1007/978-94-007-5618-2_2.
[37] J.Tennyson, Astronomical Spectroscopy: An Introduction to the Atomic and Molecular Physics of Astronomical Spectroscopy. London: Imperial College Press, 2005.
[38] C. Kulesa, Terahertz spectroscopy for astronomy: From comets to cosmology, IEEE Trans. Terahertz Sci. Technol. 1 (1) (2011) 232–240, https://doi.org/10.1109/TTHZ.2011.2159648.
[39] P. R.Bunker andP.Jensen, Molecular symmetry and Spectroscopy, Second Ed. Ottawa: NRC RESEARCH PRESS, 2012.
[40] S.F. Blaskievicz, L.H. Mascaro, Y. Zhao, F. Marken, Semiconductor photoelectroanalysis and photobioelectroanalysis: A perspective, TrAC - Trends Anal. Chem. 135 (2021) 116154, https://doi.org/10.1016/j.trac.2020.116154.
[41] K. Syrek, M. Skolarczyk, M. Zych, M. Sołtys-Mróz, G.D. Sulka, A photoelectrochemical sensor based on anodic tio2 for glucose determination, Sensors (Switzerland) 19 (22) (2019), https://doi.org/10.3390/s19224981.
[42] J. Chao, C. Fan, A photoelectrochemical sensing strategy for biomolecular detection, Sci. China Chem. 58 (5) (2015) 834, https://doi.org/10.1007/s11426-015-5402-1.
[43] J. Shu, D. Tang, Recent Advances in Photoelectrochemical Sensing: From Engineered Photoactive Materials to Sensing Devices and Detection Modes, Anal. Chem. 92 (1) (2020) 363–377, https://doi.org/10.1021/acs.analchem.9b04199.
[44] G. Wen, X. Wen, M.M.F. Choi, S. Shuang, Photoelectrochemical sensor for detecting Hg2+ based on exciton trapping, Sensors Actuators B Chem. 221 (2015) 1449–1454, https://doi.org/10.1016/j.snb.2015.07.103.
[45] N. Thomas, V. Singh, S. Kuss, Optical fibers in analytical electrochemistry: Recent developments in probe design and applications, TrAC - Trends Anal. Chem. 136 (2021) 116196, https://doi.org/10.1016/j.trac.2021.116196.
[46] N. Kaval, C.J. Seliskar, W.R. Heineman, Spectroelectrochemical Sensing Based on Multimode Selectivity Simultaneously Achievable in a Single Device. 16. Sensing by Fluorescence, Anal. Chem. 75 (22) (2003) 6334–6340, https://doi.org/10.1021/ac0347664.
[47] H.Ju, "Grand challenges in analytical chemistry: Towards more bright eyes for scientific research, social events and human health," Front. Chem., vol. 1, pp. 1–6, doi: 10.3389/fchem.2013.00005.
[48] F.W. McLafferty, "Trends in analytical instrumentation," *TrAC - Trends Anal. Chem.* Science 22 (4672) (1984) 251–253, https://doi.org/10.1126/science.6484571.
[49] K. Cammann, Sensors and analytical chemistry: Sensitivity versus quality, Phys. Chem. Chem. Phys. 5 (23) (2003) 5159–5168, https://doi.org/10.1039/b309894j.
[50] A. Bogomolov, A. Evseeva, E. Ignatiev, V. Korneev, New approaches to data processing and analysis in optical sensing, TrAC - Trends Anal. Chem. 160 (2023) 116950, https://doi.org/10.1016/j.trac.2023.116950.
[51] K.L. Glenn, D. Rodgers, R.A. Lodder, C.L. Banyon, Using the Internet as an analytical instrument, TrAC - Trends Anal. Chem. 20 (5) (2001) 219–224, https://doi.org/10.1016/S0165-9936(01)00057-7.
[52] G. Wang, J. Xu, H. Chen, Progress in the studies of photoelectrochemical sensors, Sci. China, Ser. B Chem. 52 (11) (2009) 1789–1800, https://doi.org/10.1007/s11426-009-0271-0.
[53] A. Ravindran, D. Nirmal, P. Prajoon, D. Gracia Nirmala Rani, Optical Grating Techniques for MEMS-Based Spectrometer-A Review, IEEE Sens. J. 21 (5) (2021) 5645–5655, https://doi.org/10.1109/JSEN.2020.3041196.
[54] S.L. Karsten, M.C. Tarhan, L.C. Kudo, D. Collard, H. Fujita, Point-of-care (POC) devices by means of advanced MEMS, Talanta 145 (2015) 55–59, https://doi.org/10.1016/j.talanta.2015.04.032.
[55] J. H.Nichols, "Point-of-care testing," in Contemporary Practice in Clinical Chemistry, INC, 2020, pp. 323–336. doi: 10.1016/B978-0-12-815499-1.00019-3.
[56] Z. Yu, C. Qiu, L. Huang, Y. Gao, D. Tang, Microelectromechanical Microsystems-Supported Photothermal Immunoassay for Point-of-Care Testing of Aflatoxin B1 in Foodstuff, Anal. Chem. 95 (8) (2023) 4212–4219, https://doi.org/10.1021/acs.analchem.2c05617.
[57] V. Turbé, et al., Towards an ultra-rapid smartphone- connected test for infectious diseases, Sci. Rep. 7 (11971) (2017) 1–11, https://doi.org/10.1038/s41598-017-11887-6.
[58] G.T. Hansen, Point-of-care testing in microbiology: A mechanism for improving patient outcomes, Clin. Chem. 66 (1) (2020) 124–137, https://doi.org/10.1373/clinchem.2019.304782.
[59] M. Xie, T. Chen, Z. Cai, B. Lei, C. Dong, An All-in-One Platform for On-Site Multiplex Foodborne Pathogen Detection Based on Channel-Digital Hybrid Microfluidics, Biosensors 14 (1) (2024), https://doi.org/10.3390/bios14010050.
[60] K.A. Bauer, K.K. Perez, G.N. Forrest, D.A. Goff, Review of rapid diagnostic tests used by antimicrobial stewardship programs, Clin. Infect. Dis. 59 (Suppl 3) (2014) S134–S145, https://doi.org/10.1093/cid/ciu547.
[61] M. Plebani, G. Lippi, Point of care testing: Evolving scenarios and innovative perspectives, Clin. Chem. Lab. Med. 52 (3) (2014) 309–311, https://doi.org/10.1515/cclm-2013-0654.
[62] V.M.T. Lattanzio, et al., Evaluation of mycotoxin screening tests in a verification study involving first time users, Toxins (Basel). 11 (2) (2019) 1–18, https://doi.org/10.3390/toxins11020129.
[63] Y. Liu, et al., Chromatographic methods for rapid aflatoxin B1 analysis in food: A review, Crit. Rev. Food Sci. Nutr. 64 (16) (2024) 5515–5532, https://doi.org/10.1080/10408398.2022.2155107.
[64] H. Gou, J. Zhang, M. Liao, Editorial: Point-of-care testing for infectious and foodborne pathogens, Front. Cell. Infect. Microbiol. 12 (July) (2022) 10–12, https://doi.org/10.3389/fcimb.2022.975449.
[65] I.A. Quintela, T. Vasse, C.S. Lin, V.C.H. Wu, Advances, applications, and limitations of portable and rapid detection technologies for routinely encountered foodborne pathogens, Front. Microbiol. 13 (December) (2022), https://doi.org/10.3389/fmicb.2022.1054782.
[66] M.W. Tyndall, et al., Leukocyte esterase-urine strips for the screening of men with urethritis - Use in developing countries, Genitourin. Med. 70 (1) (1994) 3–6, https://doi.org/10.1136/sti.70.1.3.
[67] J.M. Sheele, et al., Vaginal leukocyte counts for predicting sexually transmitted infections in the emergency department, Am. J. Emerg. Med. 49 (2021) 373–377, https://doi.org/10.1016/j.ajem.2021.06.070.
[68] J.O.N. Lundberg, S. Carlsson, L. Engstrand, E. Morcos, N.P. Wiklund, E. Weitzberg, Urinary nitrite: More than a marker of infection, Urology 50 (2) (1997) 189–191, https://doi.org/10.1016/S0090-4295(97)00257-4.
[69] G.P. James, K.L. Paul, J.B. Fuller, Urinary Nitrite and Urinary-tract Infection, Am. J. Clin. Pathol. 70 (4) (1978) 671–678, https://doi.org/10.1093/ajcp/70.4.671.
[70] Y.-Q. Han, L. Zhang, J.-R. Wang, S.-C. Xu, Z.-D. Hu, Net benefit of routine urine parameters for urinary tract infection screening: a decision curve analysis, Ann. Transl. Med. 8 (9) (2020), https://doi.org/10.21037/atm.2019.09.52, 601–601.
[71] A.R. Hamoud, L. Weaver, D.E. Stec, T.D. Hinds, Bilirubin in the Liver–Gut Signaling Axis, Trends Endocrinol. Metab. 29 (3) (2018) 140–150, https://doi.org/10.1016/j.tem.2018.01.002.
[72] Z.J. Khitan, R.J. Glassock, Foamy Urine: Is This a Sign of Kidney Disease? Clin. J. Am. Soc. Nephrol. 14 (11) (2019) 1664–1666, https://doi.org/10.2215/CJN.06840619.
[73] D. D.Chiras, Human Biology, 9th ed. Jones & Bartlett Learning, 2019.
[74] J. Zhou, et al., Polymeric microsphere enhanced surface plasmon resonance imaging immunosensor for occult blood monitoring, Sensors Actuators B Chem. 350 (2022) 130858, https://doi.org/10.1016/j.snb.2021.130858.
[75] N. Goto, Y. Nagaoka, K. Watanabe, Y. Miyaoka, M. Nagai, Y. Kanno, Clinical Study of the Effects of Menstrual Blood on Proteinuria, J. Tokyo Med. Univ. 79 (1) (2021) 28–54.

[76] H. Çelik, B.B. Caf, C. Geyik, G. Çebi, M. Tayfun, Enhancing urinalysis with smartphone and AI: A Comprehensive Review of Point-of-Care Urinalysis and Nutritional Advice, Chem. Pap. (2023) 1–14, https://doi.org/10.1007/s11696-023-03137-z.
[77] J.R. Kuiper, K.M. O'Brien, K.K. Ferguson, J.P. Buckley, Urinary specific gravity measures in the U.S. population: Implications for the adjustment of non-persistent chemical urinary biomarker data, Environ. Int. 156 (2021) 106656, https://doi.org/10.1016/j.envint.2021.106656.
[78] W. Mao, et al., Relationship between urine specific gravity and the prevalence rate of kidney stone, Transl. Androl. Urol. 10 (1) (2021) 184–194, https://doi.org/10.21037/TAU-20-929.
[79] J.C. Newman, E. Verdin, Ketone Bodies as Signaling Metabolites, Trends Endocrinol Metab 25 (1) (2014) 42–52, https://doi.org/10.1016/j.tem.2013.09.002.
[80] A. Wang, et al., Urine ketone bodies and adverse outcomes in patients with acute ischemic stroke or TIA, Atheroscler. Plus 48 (2022) 20–26, https://doi.org/10.1016/j.athplu.2022.03.001.
[81] K. Yamahara, M. Yasuda-Yamahara, S. Kuwagata, M. Chin-Kanasaki, S. Kume, Ketone Body Metabolism in Diabetic Kidney Disease, Kidney360 5 (2) (2024) 320–326, https://doi.org/10.34067/KID.0000000000000359.
[82] P.V. Röder, B. Wu, Y. Liu, W. Han, Pancreatic regulation of glucose homeostasis, Exp. Mol. Med. 48 (November 2015) (2016) e219, https://doi.org/10.1038/emm.2016.6.
[83] D.K. Song, Y.S. Hong, Y.A. Sung, H. Lee, Association of serum creatinine levels and risk of type 2 diabetes mellitus in Korea: a case control study, BMC Endocr. Disord. 22 (1) (2022) 1–7, https://doi.org/10.1186/s12902-021-00915-2.
[84] H.Y. Wu, et al., Diagnostic performance of random urine samples using albumin concentration vs ratio of albumin to creatinine for microalbuminuria screening in patients with diabetes mellitus: A systematic review and meta-analysis, JAMA Intern. Med. 174 (7) (2014) 1108–1115, https://doi.org/10.1001/jamainternmed.2014.1363.
[85] O. Abid, Q. Sun, K. Sugimoto, D. Mercan, J.L. Vincent, Predictive value of microalbuminuria in medical ICU patients: Results of a pilot study, Chest 120 (6) (2001) 1984–1988, https://doi.org/10.1378/chest.120.6.1984.
[86] J.L. Parker, et al., Reliability of urinalysis for identification of proteinuria is reduced in the presence of other abnormalities including high specific gravity and hematuria, Urol. Oncol. Semin. Orig. Investig. 38 (11) (2020), https://doi.org/10.1016/j.urolonc.2020.06.035, 853.e9-853.e15.
[87] P.E. Stevens, A. Levin, Evaluation and Management of Chronic Kidney Disease: Synopsis of the Kidney Disease: Improving Global Outcomes 2012 Clinical Practice Guideline, Ann. Intern. Med. 158 (11) (2013) 825–831, https://doi.org/10.7326/0003-4819-158-11-201306040-00007.
[88] S.I. Hallan, E. Ritz, S. Lydersen, S. Romundstad, K. Kvenild, S.R. Orth, Combining GFR and albuminuria to classify CKD improves prediction of ESRD, J. Am. Soc. Nephrol. 20 (5) (2009) 1069–1077, https://doi.org/10.1681/ASN.2008070730.
[89] P. Delanaye, E.P. Cohen, Formula-based estimates of the GFR: equations variable and uncertain, Nephron Clin. Pract. 110 (1) (2008), https://doi.org/10.1159/000151436.
[90] A.C. Webster, E.V. Nagler, R.L. Morton, P. Masson, Chronic Kidney Disease, Lancet 389 (10075) (2017) 1238–1252, https://doi.org/10.1016/S0140-6736(16)32064-5.
[91] National Kidney Fondation, GFR (Glomerular Filtration Rate): A Key to Understanding How Well Your Kidneys Are Working, Natl. Kidney Found (2013) 1–16 [Online]. Available: https://www.kidney.org/sites/default/files/docs/11-10-1813_abe_patbro_gfr_b.pdf.
[92] K.U. Eckardt, et al., Improving the prognosis of patients with severely decreased glomerular filtration rate (CKD G4+): conclusions from a Kidney Disease: Improving Global Outcomes (KDIGO) Controversies Conference, Kidney Int 93 (6) (2018) 1281–1292, https://doi.org/10.1016/j.kint.2018.02.006.
[93] J. Cho, J.H. Park, J.K. Kim, E.F. Schubert, White light-emitting diodes: History, progress, and future, Laser Photonics Rev. 11 (2) (2017) 1–17, https://doi.org/10.1002/lpor.201600147.
[94] B. G.Lipták, Process Control and Optimization: Instrument Engineers' Handbook, Vol. 2, 4th ed. 2006.
[95] P.G. Ellingsen, N.K. Reitan, B.D. Pedersen, M. Lindgren, Hyperspectral analysis using the correlation between image and reference, J. Biomed. Opt. 18 (3) (2013) 035001, https://doi.org/10.1117/1.JBO.18.2.020501, 1-3.
[96] H. Zaglmayr, C.G. Hu, L.D. Sun, P. Zeppenfeld, Optical referencing in differential reflectance spectroscopy, Meas. Sci. Technol. 25 (11) (2014), https://doi.org/10.1088/0957-0233/25/11/115603.
[97] F.C. DaConceição, P.P. Borges, J.F.S. Gomes, Fundamental studies to develop certified reference material to calibrate spectrophotometer in the ultraviolet region, J. Phys. Conf. Ser. 733 (1) (2016), https://doi.org/10.1088/1742-6596/733/1/012016.
[98] M. Lam, et al., Short-term thermal-humidity shock affects point-of-care glucose testing: Implications for health professionals and patients, J. Diabetes Sci. Technol. 8 (1) (2014) 83–88, https://doi.org/10.1177/1932296813514325.
[99] S. Neumann, K. Fechner, C.P. Czerny, Stability of canine urine samples under different storage conditions, Can. J. Vet. Res. 84 (4) (2020) 259–264.
[100] W.H. Chiu, et al., Using an ultra-compact optical system to improve lateral flow immunoassay results quantitatively, Heliyon 8 (12) (2022) e12116, https://doi.org/10.1016/j.heliyon.2022.e12116.
[101] D. C.Harris, Quantitative Chemical Analysis, 8th ed. New York: W. H. Freeman and Company, 2010.